NASA TM SX-727

TECHNICAL MEMORANDUM

SX-727

for the

U.S. Army

SUMMARY OF RESULTS OBTAINED IN FULL-SCALE TUNNEL INVESTIGATION OF THE RYAN FLEX-WING AIRPLANE

By Joseph L. Johnson, Jr., and James L. Hassell, Jr.

Langley Research Center
Langley Station, Hampton, Va.

NATIONAL AERONAUTICS AND SPACE ADMINISTRATION
WASHINGTON

AUG 14 1962

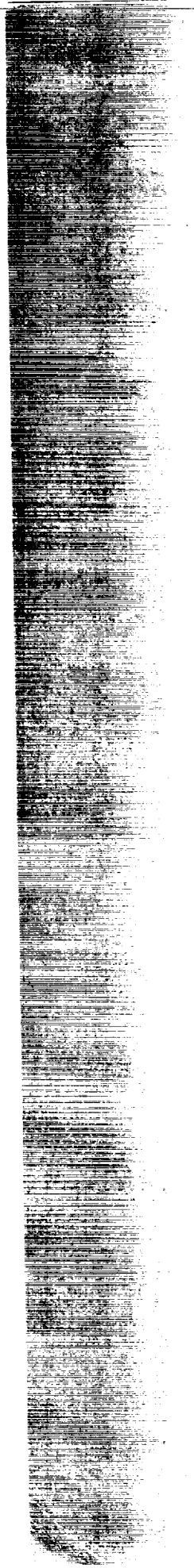

NATIONAL AERONAUTICS AND SPACE ADMINISTRATION

TECHNICAL MEMORANDUM SX-727

for the

U.S. Army

SUMMARY OF RESULTS OBTAINED IN FULL-SCALE TUNNEL INVESTIGATION OF THE RYAN FLEX-WING AIRPLANE

By Joseph L. Johnson, Jr., and James L. Hassell, Jr.

ABSTRACT

The performance and static stability and control characteristics of the Ryan Flex-Wing airplane were determined in an investigation conducted in the Langley full-scale tunnel through an angle-of-attack range of the keel from about 14° to 44° for power-on and -off conditions. Comparisons of the wind-tunnel data with flight-test data obtained with the same airplane by the Ryan Aeronautical Company were made in a number of cases.

NATIONAL AERONAUTICS AND SPACE ADMINISTRATION

TECHNICAL MEMORANDUM SX-727

for the

U.S. Army

SUMMARY OF RESULTS OBTAINED IN FULL-SCALE TUNNEL INVESTIGATION OF THE RYAN FLEX-WING AIRPLANE

By Joseph L. Johnson, Jr., and James L. Hassell, Jr.

SUMMARY

An investigation has been conducted in the Langley full-scale tunnel to determine the performance and stability and control characteristics of the Ryan Flex-Wing airplane. The tunnel tests showed that the maximum lift coefficient of the airplane occurred at a keel angle of attack of 42° and was 1.24 with power off and 1.33 with power on. The maximum lift-drag ratio was about 5.5. With stick fixed, the airplane had about neutral static longitudinal stability below 20° keel angle of attack, a moderate degree of stability from 20° to 35°, and longitudinal instability, or pitch-up, from 35° to 42°. At 42° angle of attack of the keel the airplane again became stable. With stick free, the longitudinal stability was generally worse with the airplane being only about neutrally stable between 20° to 35° angle of attack. The airplane, in general, was directionally stable and had positive effective dihedral throughout the angle-of-attack range investigated. The lateral control provided by banking the wing did not appear to be satisfactory because of inadequate rolling moments and excessively high stick forces. Analysis of the tunnel data indicated that the rudder was a better roll-control device with power on (inasmuch as the rudder is in the slipstream of the pusher propeller) than the wing-bank control system provided on the airplane. The rudder was not very effective with power off.

INTRODUCTION

An investigation has been conducted in the Langley full-scale tunnel to determine the performance and stability and control characteristics of the Ryan Flex-Wing airplane. This airplane is a simplified research machine which consists basically of a cargo platform attached to a parawing by means of an overhead-truss arrangement. The vehicle is powered by a pusher propeller located at the rear of the platform

and has a cockpit located at the front. Control is obtained by banking or pitching the wing with respect to the cargo platform. A rudder operating in the propeller slipstream provides directional control.

The investigation consisted of static force tests made over an angle-of-attack range of the keel from about 14° to 44° to measure the basic aerodynamic and longitudinal and lateral stability and control characteristics of the airplane with power off and on. In addition to the basic control tests, the airplane was also tested with an alternative lateral control system in which the aft portion of each leading edge of the parawing was deflected laterally to provide roll control.

The most significant results of the investigation have been summarized and are presented herein. Comparisons of the wind-tunnel data with flight-test data obtained by the Ryan Aeronautical Company (ref. 1) have been made in a number of cases.

A three-view drawing of the airplane and photographs of the airplane mounted for force testing in the Langley full-scale tunnel are shown in figures 1 and 2, respectively. The results of the investigation are presented in figures 3 to 21.

SYMBOLS

All forces, moments, and velocities are presented with respect to the stability-axis system which originates at the reference center-of-gravity position shown in figure 1. All measurements are reduced to coefficient form and are based on the dimensional characteristics of the fully developed wing (45° leading-edge sweep).

b	wing span, ft
c_k	keel length, ft
C_D	drag coefficient, F_D/qS
C_h	hinge-moment coefficient, M_h/qSb for roll, M_h/qSc_k for pitch
C_l	rolling-moment coefficient, M_X/qSb
C_L	lift coefficient, F_L/qS
C_m	pitching-moment coefficient, M_Y/qSc_k

C_n yawing-moment coefficient, M_Z/qSb

C_Y lateral-force coefficient, F_Y/qS

$C_{l_p} = \frac{\partial C_l}{\partial \frac{pb}{2V}}$, per radian

$C_{l_\beta} = \frac{\partial C_l}{\partial \beta}$, per deg

$C_{n_\beta} = \frac{\partial C_n}{\partial \beta}$, per deg

$C_{Y_\beta} = \frac{\partial C_Y}{\partial \beta}$, per deg

ΔC_m incremental pitching-moment coefficient

$\frac{\partial C_m}{\partial C_L}$ slope of pitching-moment curve with lift coefficient

F_D drag, lb

F_L lift, lb

F_Y side force, lb

g acceleration due to gravity, 32 ft/sec^2

i_w angle of incidence of parawing keel with respect to platform, $\alpha_k - \alpha$, deg

L/D lift-drag ratio

M_h hinge moment, ft-lb

M_X rolling moment, ft-lb

M_Y pitching moment, ft-lb

M_Z yawing moment, ft-lb

p	rolling velocity, radians/sec
q	free-stream dynamic pressure, lb/sq ft
S	wing area, sq ft
T_c	thrust coefficient, $\left[C_D \text{ (power on)} - C_D \text{ (power off, propeller stopped)}\right]_{\alpha=0^\circ}$
V	free-stream velocity, ft/sec
W	weight, lb
W/S	wing loading, lb/sq ft
x, z	horizontal and vertical distance from airplane center of gravity to wing pivot, respectively, ft
α	angle of attack of platform, deg
α_k	angle of attack of keel, deg
β	angle of sideslip, deg
δ_r	rudder deflection, deg
δ_t	wing-tip deflection, deg
φ	angle of roll, positive when right wing tip is down, deg

LONGITUDINAL CHARACTERISTICS

The lift, drag, L/D, and longitudinal stability and control characteristics of the airplane are summarized in figures 3 to 16.

Basic longitudinal data for the airplane are plotted in figures 3 and 4 for the power-off and power-on conditions for three wing incidences which cover the wing-incidence range available in the flight tests conducted by the Ryan Aeronautical Company. The power-off tests were made with the propeller stopped, and no tests were made with the propeller removed. Inasmuch as the drag of the stopped propeller was probably very small, it was arbitrarily assumed that the thrust coefficient T_c was zero for the power-off tests. The data of figure 3 are plotted against the angle of attack of the wing keel, and the data for figure 4 are plotted against platform angle of attack. The 25° incidence was

considered the basic condition in the force tests, and most of the tests were run with this incidence. The data of figures 3 and 4 were obtained with the dynamic pressure held constant during the test run. In order to represent a 1 g flight condition (lift equal to aircraft weight), these data require certain corrections which can be made by using the data of figure 5. (In addition, to represent flight out of ground effect properly, these data should be corrected to account for the fact that the airplane was close enough to the ground board in the tunnel tests to produce small effects of ground proximity on lift, drag, and pitching moment. These ground-effect corrections are covered in the discussion of subsequent figures.)

Figure 5 presents lift, drag, and pitching-moment data for the $i_w = 25^\circ$ power-off condition obtained in tests at different values of constant dynamic pressure, ranging from 1.60 to 5.60 pounds per square foot which correspond to airspeeds of about 25 to 47 miles per hour, respectively. (The data of figs. 3 and 4, as well as most of the data presented in later figures, were obtained at a dynamic pressure of 3.07. Although the data are identified as constant q conditions, actually there was some slight reduction in q with C_L during each run. The q value listed for each run corresponds to the value measured at $\alpha = 0^\circ$.) The data of figure 5 do not show a consistent effect of test dynamic pressure on lift and drag but do show a consistently greater negative pitching moment with increasing dynamic pressure. The heavy dashed curve intersecting the pitching-moment curves of figure 5 represents the pitching moments for a 1 g flight condition. This curve was obtained from the basic relationship $C_L = \frac{W/S}{q}$ (or $qC_L = W/S$) by using a value of W/S of 3.32 lb/sq ft for the airplane. The heavy curve intersects each of the other curves at the lift coefficient where the product of C_L and the measured q is equal to the airplane wing loading. It is apparent that this curve for the 1 g flight condition has a flatter slope (and therefore less static longitudinal stability) than the curves obtained at the higher values of constant dynamic pressure, particularly in the low and moderate lift-coefficient range.

For ease of comparison, the pitching-moment curve for 1 g flight and the curve obtained at the constant dynamic pressure of 3.07 used in most of the tunnel tests are replotted in figure 6. Inasmuch as the effects of dynamic pressure were determined only for the $i_w = 25^\circ$ power-off condition, the pitching-moment data for other test conditions were corrected to 1 g conditions by using the increments between the two pitching-moment curves in figure 6. Data corrected in this manner for the various wing incidence and power conditions covered in figure 4 are presented in figure 7.

The lift curves in figure 7 appear to be normal with a lift-curve slope slightly greater than 0.05 per degree with power on and slightly less than 0.05 with power off. Maximum lift coefficient, which is obtained at a keel angle of attack of about 42° is 1.24 with power off and 1.33 with power on. Although data are shown for angles of attack of the keel as low as 14°, it was noted during the tests that trailing-edge flutter occurred at keel angles of attack below about 27° and that the flutter became progressively worse as the angle of attack was reduced. Because of the severe flutter at angles of attack below about 20°, it appears that it would be undesirable to operate the aircraft at angles of attack below this value. Figure 8 shows fairly good agreement between flight and in the force tests. The force-test lift coefficients measured in flight and in the force tests. The force-test lift curve in figure 8 is an average of the power-on lift curves in figure 7.

Figure 7 shows that the maximum L/D of the airplane is about 5.5 and is obtained at about 27° or 28° keel angle of attack. An estimate of the L/D of about 7 for the wing alone was made from the data of figure 7 together with data for the platform alone.

The pitching-moment data in figure 7 show about neutral static longitudinal stability below 20° keel angle of attack, a moderate degree of stability from 20° to 35°, and longitudinal instability, or pitch-up, from 35° to 42°. At 42° the data of figure 7(c) indicate a stabilizing break in the pitching-moment curve. The amount of static margin the airplane has in the stable range will be indicated in a subsequent figure.

As pointed out previously, the airplane probably experienced ground effects on lift, drag, and pitching moment in the tunnel tests. Although there are no methods available for making accurate corrections to the data for this ground effect, a general indication of the magnitude of the effect can be obtained from previous investigations with delta-wing models in and out of the presence of the ground. The results of these studies would indicate that the Flex-Wing airplane in the full-scale tunnel tests experienced slightly higher values of lift-curve slope and L/D, and slightly more negative values of C_m than it would experience out of ground effect. It appears that any corrections for the effect of the ground on lift-curve slope and L/D would be very small. The effect of the ground on C_m, however, may be more significant inasmuch as it may involve corrections as large as $\Delta C_m = 0.01C_L$ or $0.02C_L$, and such corrections could greatly affect the longitudinal trim characteristics of the airplane discussed subsequently.

The hinge-moment coefficients of the wing in pitch measured about the pivot are presented in figure 9 as determined in test runs at constant dynamic pressure. Figure 10 presents hinge-moment data for the $i_w = 25°$ power-off condition measured at various dynamic pressures. As in figure 5, a heavy dashed curve has been superimposed on the other curves

of figure 10 to represent the 1 g flight condition. The incremental hinge moments between the 1 g and $q = 3.07$ cases in figure 10 were used to correct the data of figure 9 to 1 g conditions, and the corrected data are presented in figure 11. The data for the power-on conditions of figure 11 are plotted together at the top of figure 12, and the stick forces corresponding to these hinge moments are shown in the lower plot. In view of the differences in the shape of these stick-force curves (which can be attributed to normal scatter of data) an average curve representative of the measured stick forces for all three wing incidences should be used rather than the individual curves.

In figure 13 the static margin $\left(\partial C_m/\partial C_L\right)$ and stick forces determined in the tunnel tests are compared with values measured in flight. The left-hand plots show tunnel data uncorrected for ground effect while the right-hand plots indicate the effect of two assumed values of ground-effect correction: $\Delta C_m = 0.01 C_L$ and $\Delta C_m = 0.02 C_L$. Force-test data on delta wings in and out of ground effect have indicated that corrections of this order of magnitude may apply in the present case.

The two plots at the top in figure 13 show the stick-fixed static margin of the airplane when it is trimmed at various airspeeds as determined from the tunnel data of figure 7 and from flight data. The tunnel data show a slightly higher value of static margin than the flight-test data and indicate stick-fixed stability over a speed range from about 35 to 55 miles per hour. No effect of the ground is shown on static margin because the type of ground effect assumed $\left(\Delta C_m \text{ as a function of } C_L\right)$ changes longitudinal trim but does not change the static margin for trimmed conditions at a given lift coefficient or airspeed. Including the correction for ground effect lowers the trim airspeed for any given flight condition as indicated by the vertical lines in the plot in the upper right of figure 13.

In the lower plots of figure 13, an average stick-force curve taken from the tunnel data of figure 12 is compared with flight data taken from the Ryan flight tests. Although the flight-test data shown indicate slightly stable stick forces, there are indications in the Ryan flight log that the airplane was actually unstable or at best neutrally stable for this condition. The pilot reported that the airplane had a tendency to drift off speed at various trim settings and that essentially zero stick force was required to move the stick from full forward to full rearward position. The force-test data of figure 13 indicate a small amount of stick-free stability from about 40 to 47 miles per hour and indicate stick-free instability above and below this speed range. The tunnel data indicate very large pull forces for conditions which should be approximately trimmed according to the flight data. The pull forces are made even greater when the mass unbalance present on the airplane

(wing center of gravity ahead of pivot) is taken into account. The plot at the lower right shows the large effect that a correction of $\Delta C_m = 0.01C_L$ or $0.02C_L$ has on the stick-force characteristics. From these results it is seen that a correction of $\Delta C_m = 0.02C_L$ or greater to the tunnel data is required to provide trim in the speed range from 35 to 50 miles per hour.

It should be pointed out that, in the tunnel tests and at times in the flight tests, there were large fluctuations in both the pitch- and roll-control forces which made accurate measurement of these forces impossible. A sample of data from the control force measurements made in the tunnel tests is shown in figure 14. Fluctuations in stick force of as much as ±20 pounds were obtained and there was also a shift in the general level of the readings from one time to another. In the particular data shown in figure 14, the data represented by the solid line were obtained at the beginning of a test run at a platform angle of attack of 0° while the data for the dashed line were obtained several minutes later under presumably identical test conditions after runs had been made at higher platform angles of attack. The scatter of data shown in figure 14 certainly suggests that the average values of stick force presented in figure 13 are only approximate values which should be used with caution.

An indication of the longitudinal trim capability of the airplane with various wing incidences and fore- and aft-wing positions is presented in figure 15. The tunnel data are shown for no ground-effect correction and for the two amounts of correction illustrated earlier in figure 13. For the wing-incidence range and wing-position travel available, there appears to be ample capability for trimming at the higher speeds but only limited capability for trimming in the low-speed range, unless the ground-effect correction turns out to be fairly large. However, if $\Delta C_m = 0.02C_L$ proves to be the proper ground-effect correction factor, the lower plot of figure 15 indicates that the airplane could be trimmed to speeds below the stall.

LATERAL CHARACTERISTICS

The static lateral stability characteristics of the airplane are summarized in figure 16 and the lateral control characteristics are presented in figures 17 to 21.

Lateral Stability

The static lateral stability parameters C_{n_β} (the static directional-stability parameter) and C_{l_β} (the effective-dihedral parameter) are shown in figure 16 for the $i_w = 25^\circ$ condition with power off and on and with the rudder off and on. These data indicate that the airplane was directionally stable throughout the test angle-of-attack range except for the rudder-off conditions at the highest angles of attack. Up to about 7° angle of attack of the platform $(\alpha_K = 32^\circ)$, power is shown to increase the directional stability when the rudder is installed, but there is little effect of power on the stability with the rudder off and little effect of the rudder on stability with power off. The values of the effective-dihedral parameter are rather large and increase with increasing angle of attack. These large values of C_{l_β} appear to have important effects on the lateral control as is shown in the following section.

Lateral Control

The lateral control characteristics of the airplane are presented in figure 17 in the form of incremental rolling and yawing moments produced by banking the wing 5°. Data are shown for the $i_w = 25^\circ$ case for power off and on. In general, the data show very small rolling effectiveness and favorable yawing moments for the wing-bank control at the lower platform angles of attack. The effectiveness decreases and the yawing moments become adverse at the higher angles of attack. With power on, the rolling effectiveness is slightly greater and the yawing moments more favorable than with power off.

Figure 18 presents the wing-bank control hinge-moment coefficients and stick forces for the $i_w = 25^\circ$, power-off condition for a wing bank angle of 5°. The stick forces were computed from the hinge moments for 1 g flight conditions over the angle-of-attack range shown. The roll stick force of about 75 pounds at zero platform angle of attack is in general agreement with values measured in the flight tests.

The roll-control data presented in figures 17 and 18 were obtained in tunnel tests in which the platform of the airplane was mounted on the tunnel-support struts and remained fixed when the wing was banked. When the wing banks about an axis parallel to the wing keel as in the present case, an angle of sideslip of the wing is produced $(\sin \beta = \sin \alpha_K \sin \phi)$ and this sideslip is adverse - that is a nose-left sideslip with a right wing bank. This test condition does not exactly represent what happens in flight when the wing-bank control is used. Actually, when a roll

control is applied in flight, the wing and platform momentarily roll and sideslip in opposite directions; the amount each moves is determined by the relative inertia and the aerodynamic moments of the two. Thus the true flight condition following the abrupt deflection of the wing roll control can be represented by a case somewhere between the two extreme cases of platform fixed at zero bank and sideslip (as in the present tunnel tests) and wing fixed at zero bank and sideslip (with the platform being deflected in bank and sideslip to provide roll control).

Figure 19 shows how the rolling-, yawing-, and hinge-moment coefficients vary between the two extreme cases. In the plots of the moments against bank angle, the wing bank angle of 5° (and platform bank angle of 0°) represents the test condition used in the tunnel, while the wing bank angle of 0° (and platform bank angle of -5°) represents the wing-fixed case. For the test condition illustrated ($i_w = 25°$, $\alpha = 0°$, and 5° right wing-bank control) there is a difference of about 2° in sideslip angle between the wing and platform, with the wing being sideslipped 2° more nose left than the platform. In the C_l and C_n plots, the horizontal long dashed lines represent the effect of tilting the lift vector, and the short dashed lines represent the moments produced by the wing and platform when they sideslip. The heavy solid lines are the resultant values obtained by adding the long and short dashed lines. The tunnel-test data point is shown by the symbols at 5° wing-bank angle. The C_h plot at the right on figure 19 was constructed in a similar manner, with the long dashed line representing the hinge moments about the pivot produced by the weight of the platform and with the short dashed lines representing the aerodynamic moments about the wing pivot produced by the wing and platform when they sideslip. The agreement appears to be satisfactory between the tunnel-test data points and the resultant curves on all three plots of figure 19.

Large effects of sideslip on all the moments are indicated in figure 19 so that the results for the wing-fixed and platform-fixed conditions appear to be quite different. For example, if the tunnel tests had been run with the wing fixed at zero bank and sideslip, the results would have shown much higher rolling moments but would also have shown adverse yawing moments for the wing-bank control. Actually the overall control effectiveness should be about the same for the two cases since the yawing moments produce sideslip of the airplane (either favorable or adverse), and this sideslip, acting through the effective-dihedral parameter C_{l_β}, produces rolling moments that tend to equalize the net rolling moment acting in the two cases. Perhaps the best indication of net roll-control effectiveness shown in the plots of figure 19 is the rolling moment for the case where the yawing moment is zero. This condition occurs at the point where the wing is banked 3.5° right and the

platform 1.5° left. This proportion of initial wing bank to platform bank also appears generally reasonable on the basis of the relative inertias and the aerodynamic moments of the wing and platform.

The lateral control characteristics of the airplane are summarized in figure 20. Also presented in this figure are data for a wing-tip control system in which the aft portion of each leading edge of the parawing (referred to as the control arm in fig. 1(b)) is deflected laterally about a pivot located at the 75-percent station of the basic leading edge. In addition, estimated control characteristics are presented for the wing-bank control with negative wing dihedral added.

In the left plot of figure 20, rolling-moment coefficient C_l is plotted against roll hinge-moment coefficient C_h. The horizontal dashed line represents the value of C_l required to produce a $pb/2V$ value of 0.09, based on the relationship $\frac{pb}{2V} = \frac{C_l}{C_{l_p}}$ and assuming that the value of the damping-in-roll factor C_{l_p} is -0.15. The value of $pb/2V$ of 0.09 is the minimum value specified in the handling-qualities requirements for a light liaison airplane. This criterion is presented here merely to establish a reference for purposes of comparison and is not intended to imply that a $pb/2V$ value of 0.09 is a valid specification for parawing applications. For recovery-system applications, a much smaller value may well prove to be acceptable, whereas for utility airplane applications (which may involve flight at very low speeds in confined areas) an even larger value than 0.09 may be required. In any event, considerably more research and flight experience will be required to establish the proper criteria for the various applications envisioned for the parawing. Also indicated along the C_h scale are the hinge-moment coefficients that correspond to stick forces of 50 to 100 pounds. The solid circle at the lower right, representing the wing-bank control system installed on the airplane (for the case of $\Delta C_n = 0$), shows that 5° of wing bank requires about 70 pounds of stick force and only produces about one-third of the rolling effectiveness required by the $pb/2V = 0.09$ criterion. Calculations indicate that reducing C_{l_β} by using 18° negative geometric dihedral angle of the wing would decrease the stick force to about 45 pounds and increase the effectiveness to about one-half of the criterion value. The wing-tip control tested on the airplane appears to be quite effective, with approximately a 7° control deflection producing a $pb/2V$ value of 0.09 with only about 30 pounds of stick force.

The right-hand plot of figure 20 shows the yawing moments produced by the various roll-control arrangements. The yawing moment is zero for the wing-bank control because this condition was specifically selected

from figure 19 to give the best indication of roll effectiveness. The wing-tip control produces small favorable yawing moments with 5° deflection and adverse moments with 10° deflection. The 7° deflection required for a $pb/2V$ value of 0.09 should therefore produce no appreciable yawing moments.

The rudder effectiveness data are presented in figure 21 in the form of side force, yawing-moment and rolling-moment coefficients. The rudder was not very effective in producing yawing moments with power off but the effectiveness increased by a factor of about five with power on. The rolling moments produced by rudder deflection were negligible in both the power off and on cases. If the yawing-moment coefficient produced by 20° rudder deflection is equated to C_{n_β} for the power-on condition, then the sideslipping capability of the airplane through rudder deflection can be estimated. From the sideslip angle produced in this manner, the rolling moment produced by the wing through the effective dihedral C_{l_β} can then be estimated. Calculations made from this relationship indicated that 20° rudder deflection with power on would produce a rolling-moment coefficient of about 0.0165 for the 25° keel angle-of-attack condition. The data of figure 20 indicate that a rolling-moment coefficient of this magnitude should be adequate for providing the rolling effectiveness required by the $pb/2V = 0.09$ criterion. On this basis, it would appear that the rudder should provide a better means of roll control than the wing-bank control system provided on the airplane. The pilot made extensive use of this rolling effectiveness of the rudder in flying the airplane. It should be pointed out, however, that the roll response obtained through this indirect control is subject to appreciable time lag and other dynamic effects and therefore the control effectiveness may be considerably different for such a control system than that estimated on the basis of static derivatives alone.

SUMMARY OF RESULTS

The results of the full-scale tunnel investigation of the performance and stability and control characteristics of the Ryan Flex-Wing airplane are summarized as follows:

1. The tunnel tests showed that the maximum lift coefficient of the airplane occurred at a keel angle of attack of 42° and was 1.24 with power off and 1.33 with power on. The maximum lift-drag ratio was about 5.5.

2. With stick fixed, the airplane had about neutral static longitudinal stability below 20° keel angle of attack, a moderate degree of

stability from 20° to 35°, and longitudinal instability, or pitch-up, from 35° to 42°. At 42° angle of attack of the keel the airplane again became stable. With the stick free, the longitudinal stability was generally worse with the airplane being only about neutrally stable between 20° to 35° angle of attack.

3. The airplane, in general, was directionally stable and had positive effective dihedral throughout the angle-of-attack range investigated.

4. The lateral control provided by the wing-banking control system did not appear to be satisfactory because of inadequate rolling moments and excessively high stick forces. This result is in agreement with flight-test results.

5. Analysis of the factors contributing to the low rolling effectiveness obtained by banking the wing indicated that the use of negative geometric dihedral of the wing to reduce the high values of positive effective dihedral may be a relatively simple means of improving the effectiveness of this type of roll-control system.

6. Analysis of the tunnel data indicated that the rudder was generally a better roll-control device with power on (since the rudder is in the slipstream of the pusher propeller) than the wing-bank control system provided on the airplane. The rudder provides roll control in an indirect manner by sideslipping the airplane and making use of the large value of effective dihedral (rolling moment due to sideslip).

7. The wing-tip control device tested on the airplane (which had been developed earlier at Langley in small-scale tests) produced large rolling moments with very small stick forces.

8. Because of the large roll-control forces, the lack of stick-free longitudinal stability, and the existence of large periodic pitch and roll-control force fluctuations, it appears desirable to install an irreversible power-boost control system in the airplane prior to the flight tests at Langley.

Langley Research Center,
National Aeronautics and Space Administration,
Langley Station, Hampton, Va., June 25, 1962.

REFERENCE

1. Burich, J. H., and Everett, W. L.: Flexible-Wing Manned Test Vehicle. Rep. No. 61B131 (Contract No. DA-44-177-TC-721), Ryan Aero. Co., Dec. 18, 1961.

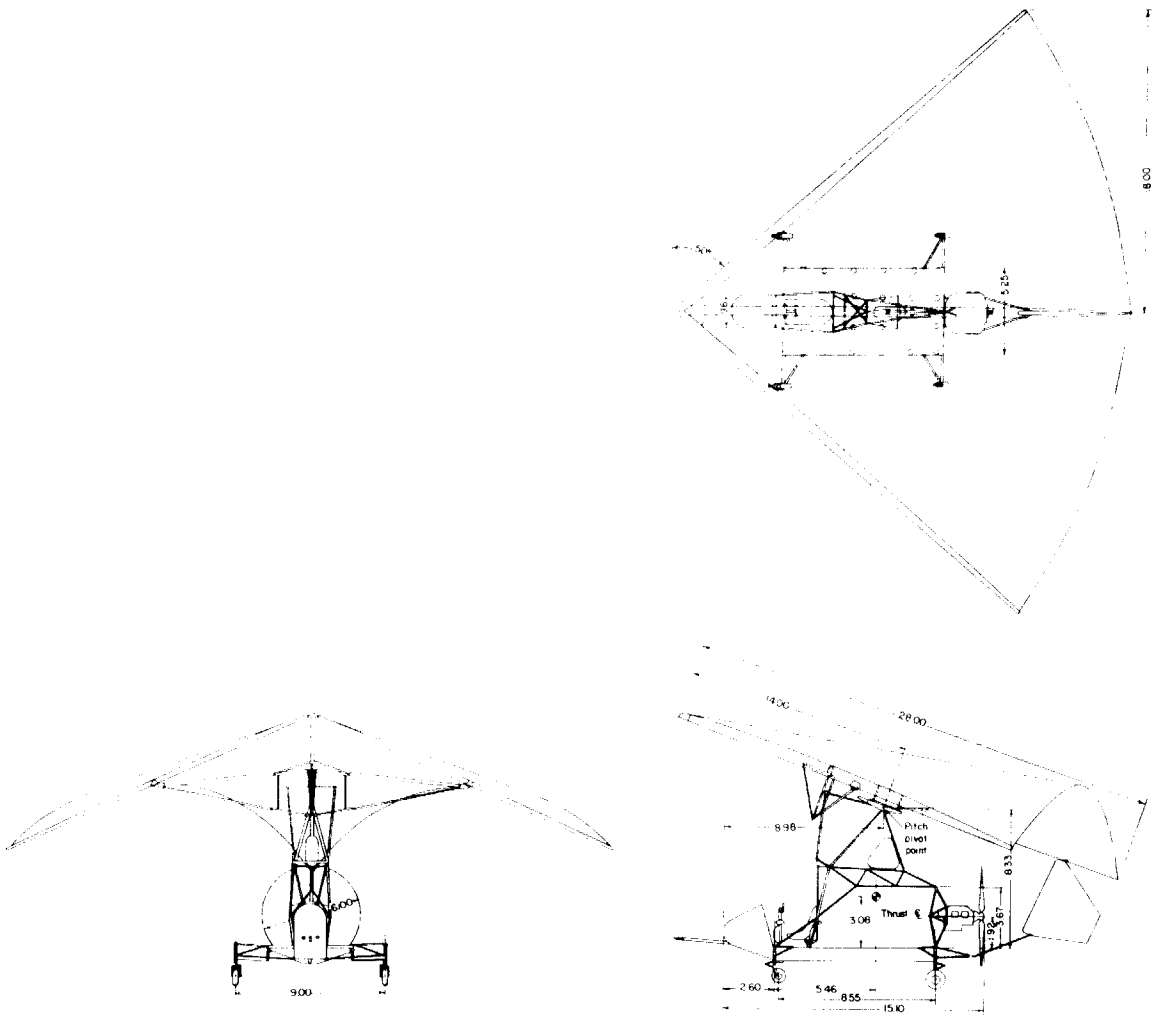

(a) Basic configuration.

Figure 1.- Three-view drawing of Ryan Flex-Wing airplane used in the investigation. All dimensions are in feet.

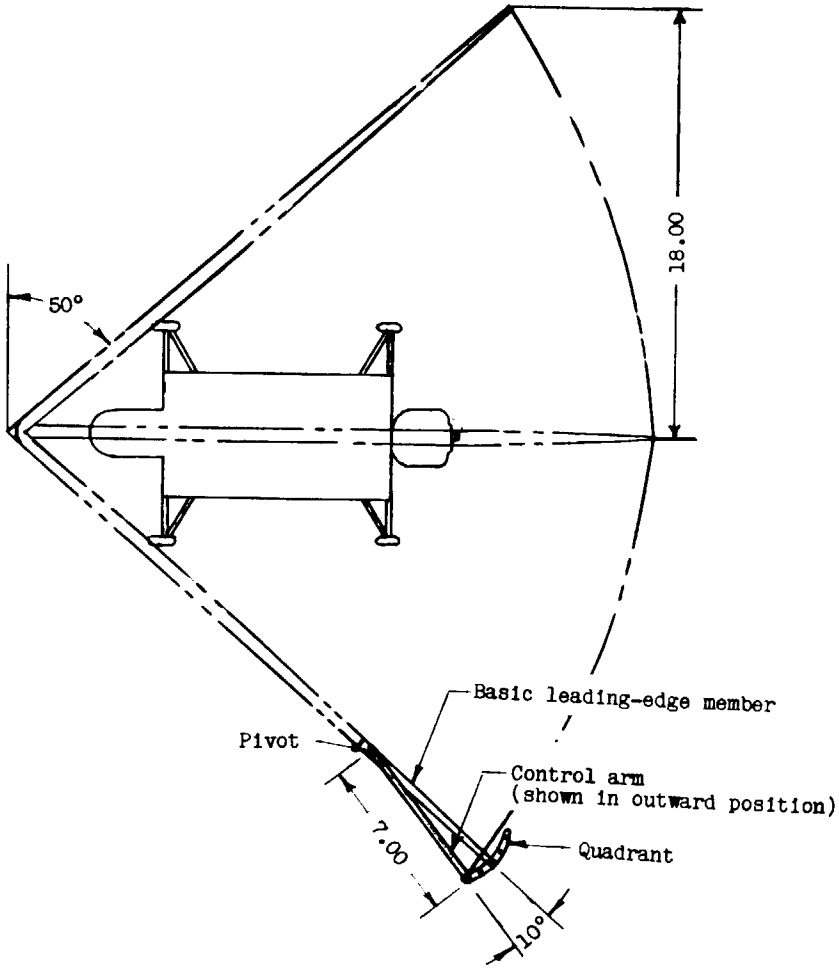

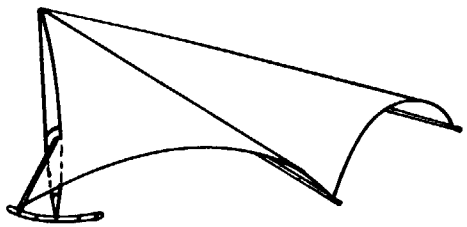

Perspective view of wing showing wing-tip control in outward position

(b) Schematic drawing of the wing-tip control system used in the investigation.

Figure 1.- Concluded.

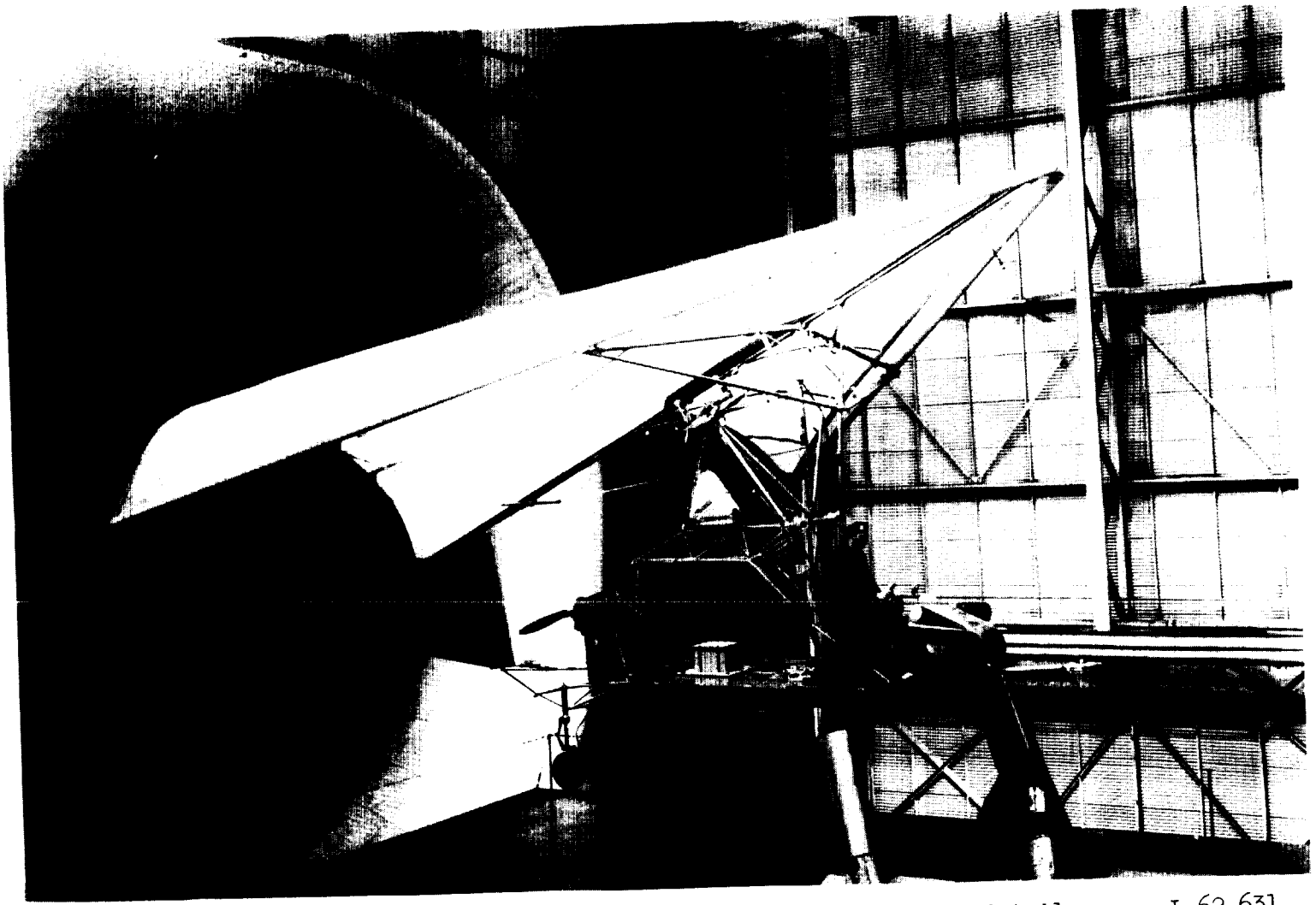

(a) Three-quarter front view showing support system details. L-62-631

Figure 2.- Photographs of Ryan Flex-Wing airplane mounted for force testing in the Langley full-scale tunnel.

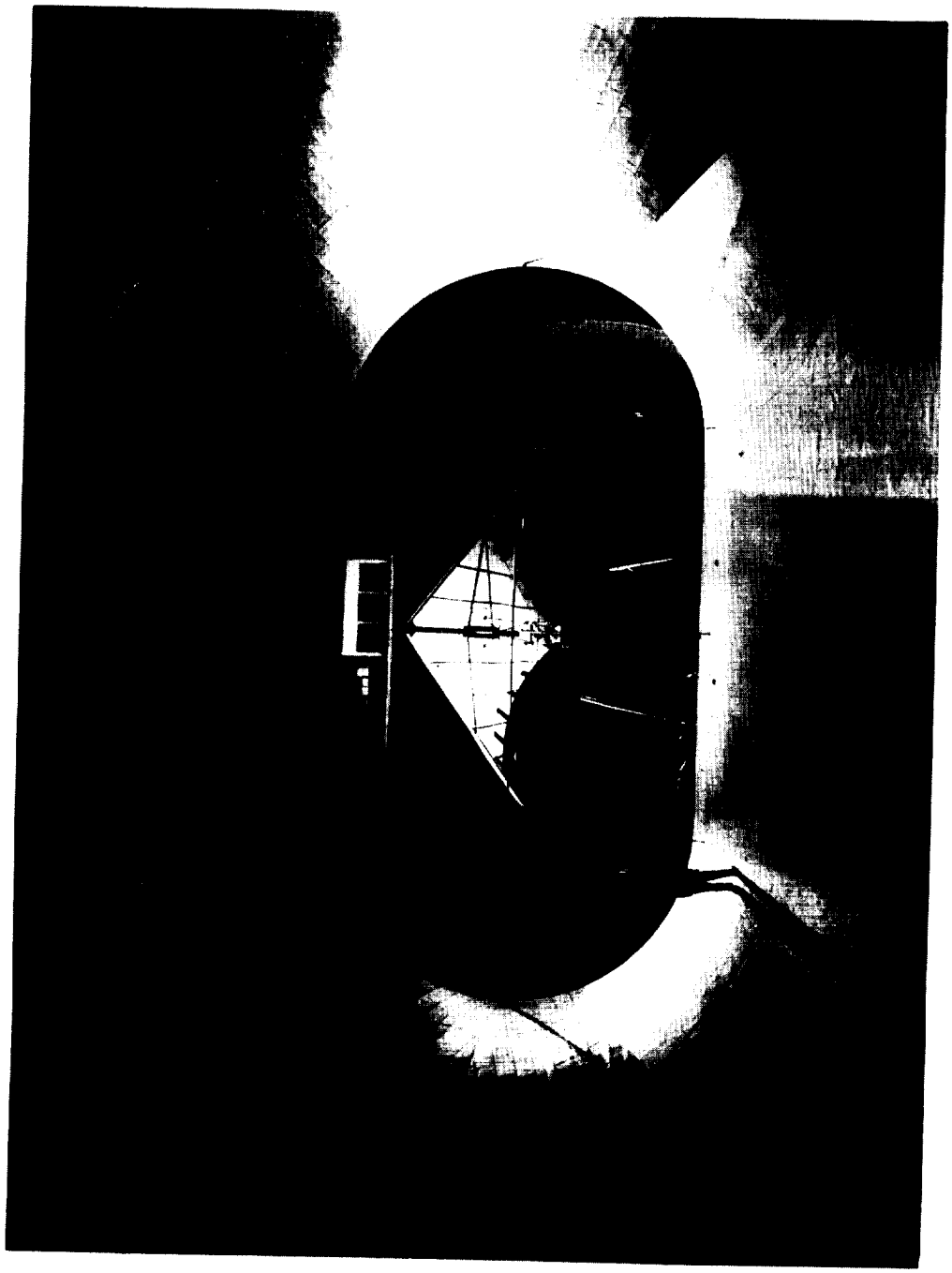

(b) Front view showing relation of airplane to test section. L-62-627

Figure 2.- Concluded.

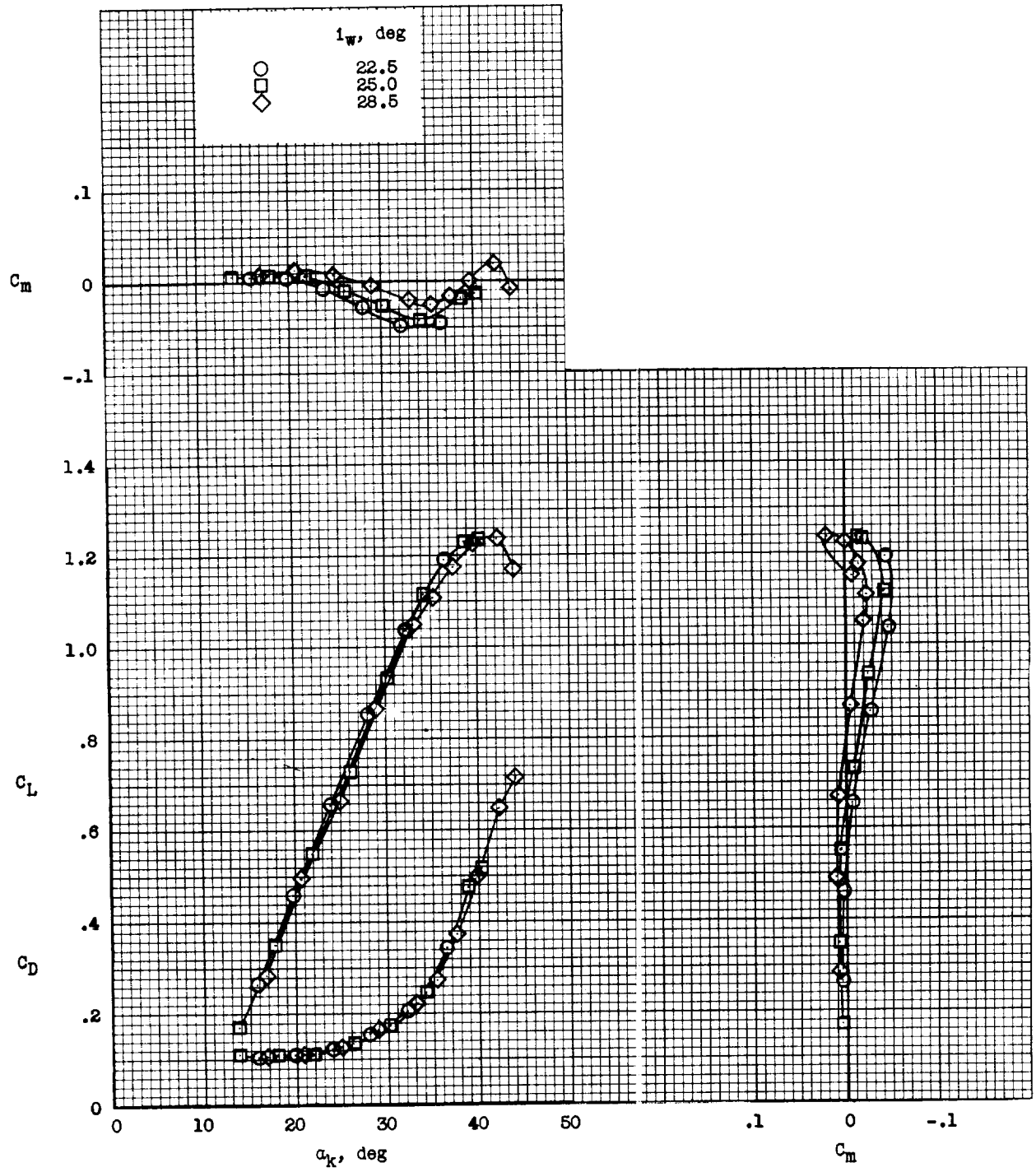

Figure 3.- Static longitudinal characteristics of the airplane. $T_c = 0$.

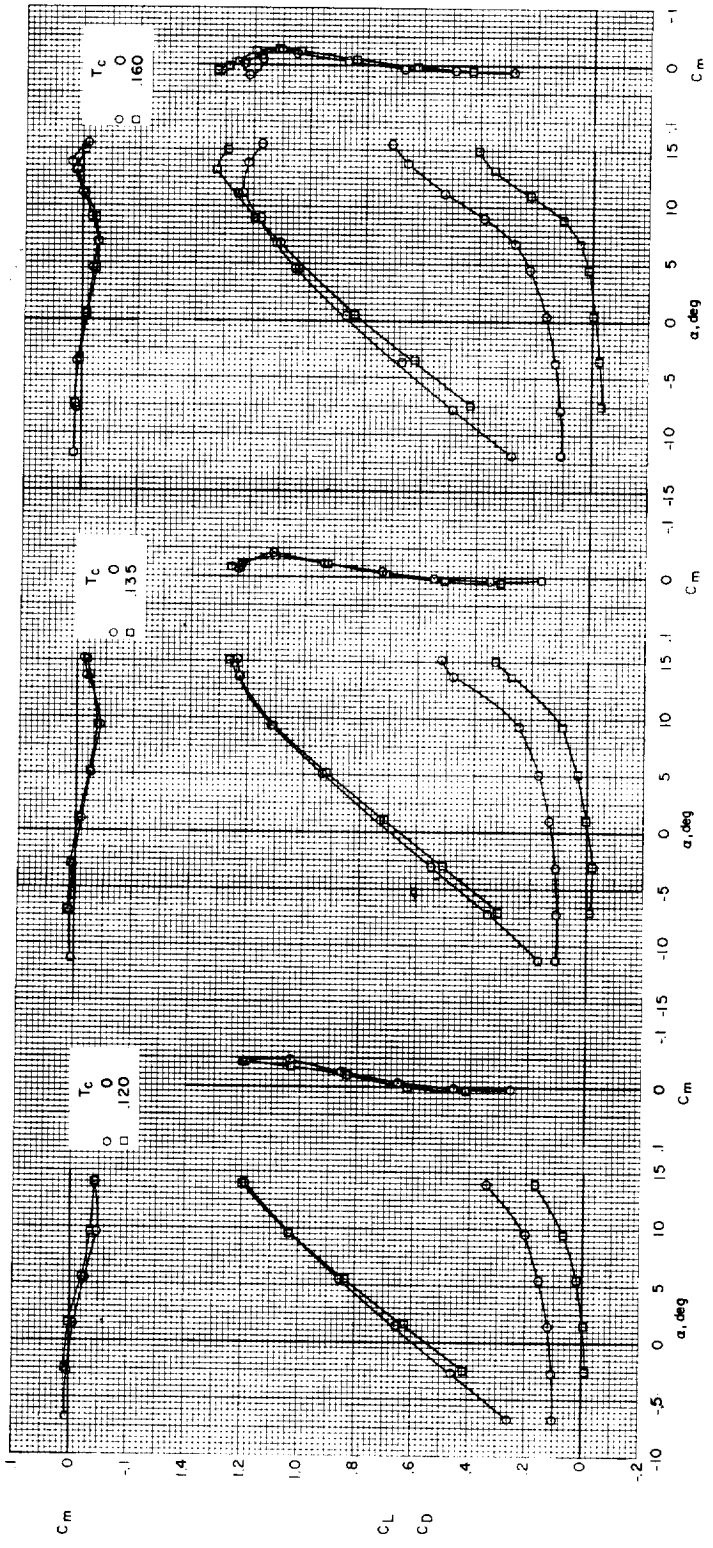

(a) $i_w = 22.5°$. (b) $i_w = 25.0°$. (c) $i_w = 28.5°$.

Figure 4.- Static longitudinal characteristics of the airplane.

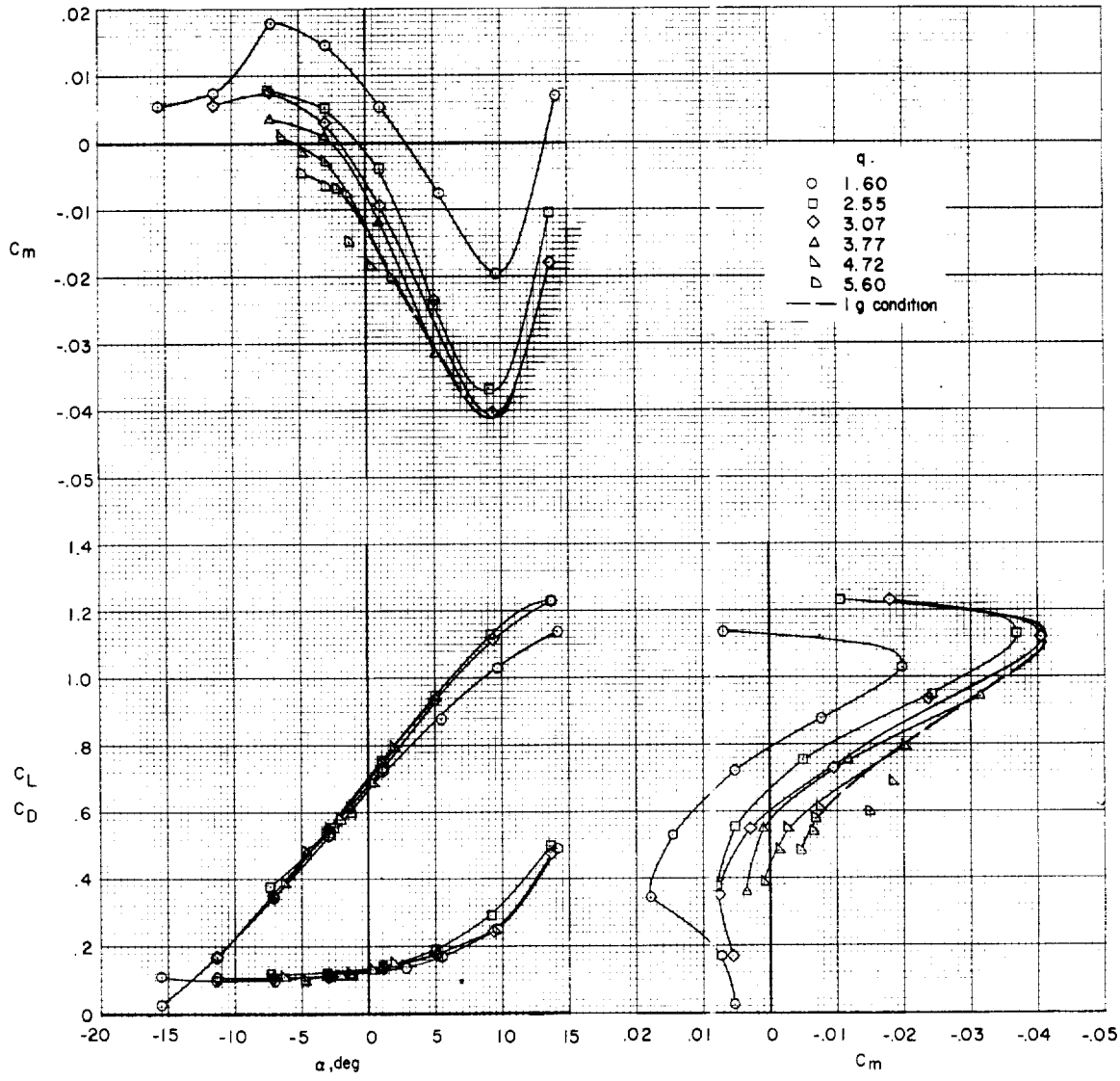

Figure 5.- Effect of dynamic pressure on the static longitudinal characteristics of the airplane. $i_w = 25°$; $T_c = 0$.

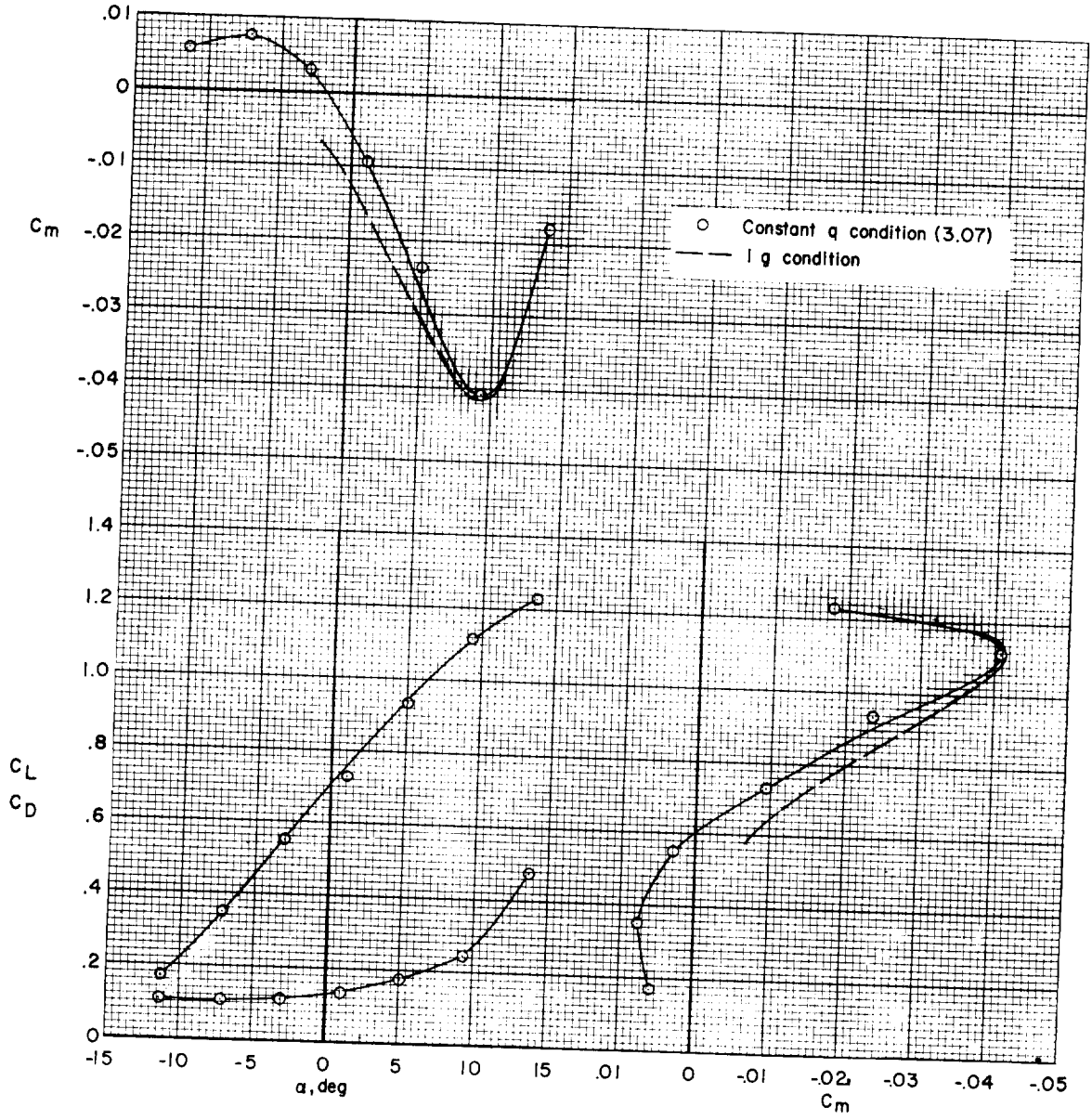

Figure 6.- Comparison of static longitudinal characteristics of the airplane for constant loading (1 g) and constant q condition. $i_w = 2.5°$; $T_c = 0$.

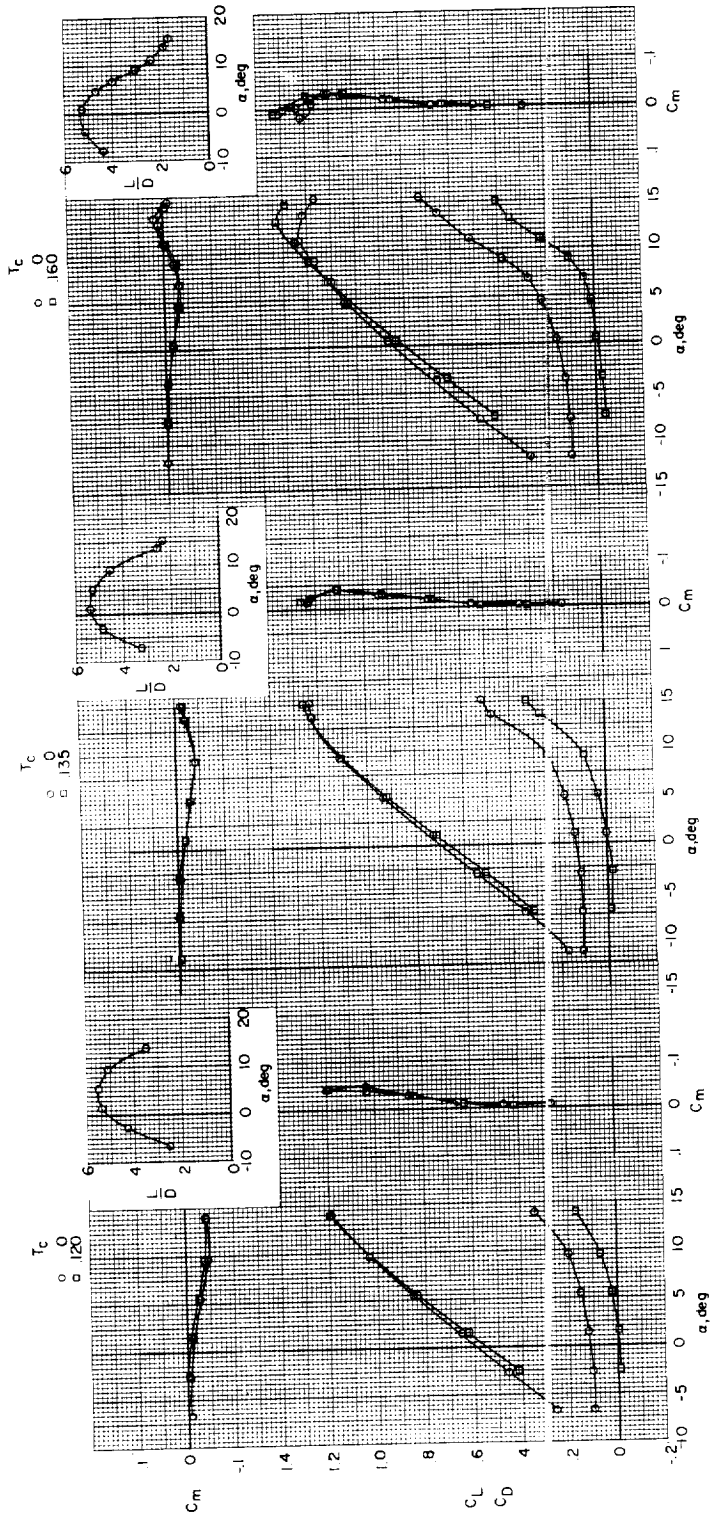

(a) $i_w = 22.5°$. (b) $i_w = 25.0°$. (c) $i_w = 28.5°$.

Figure 7.- Static longitudinal characteristics of the airplane corrected for 1 g condition.

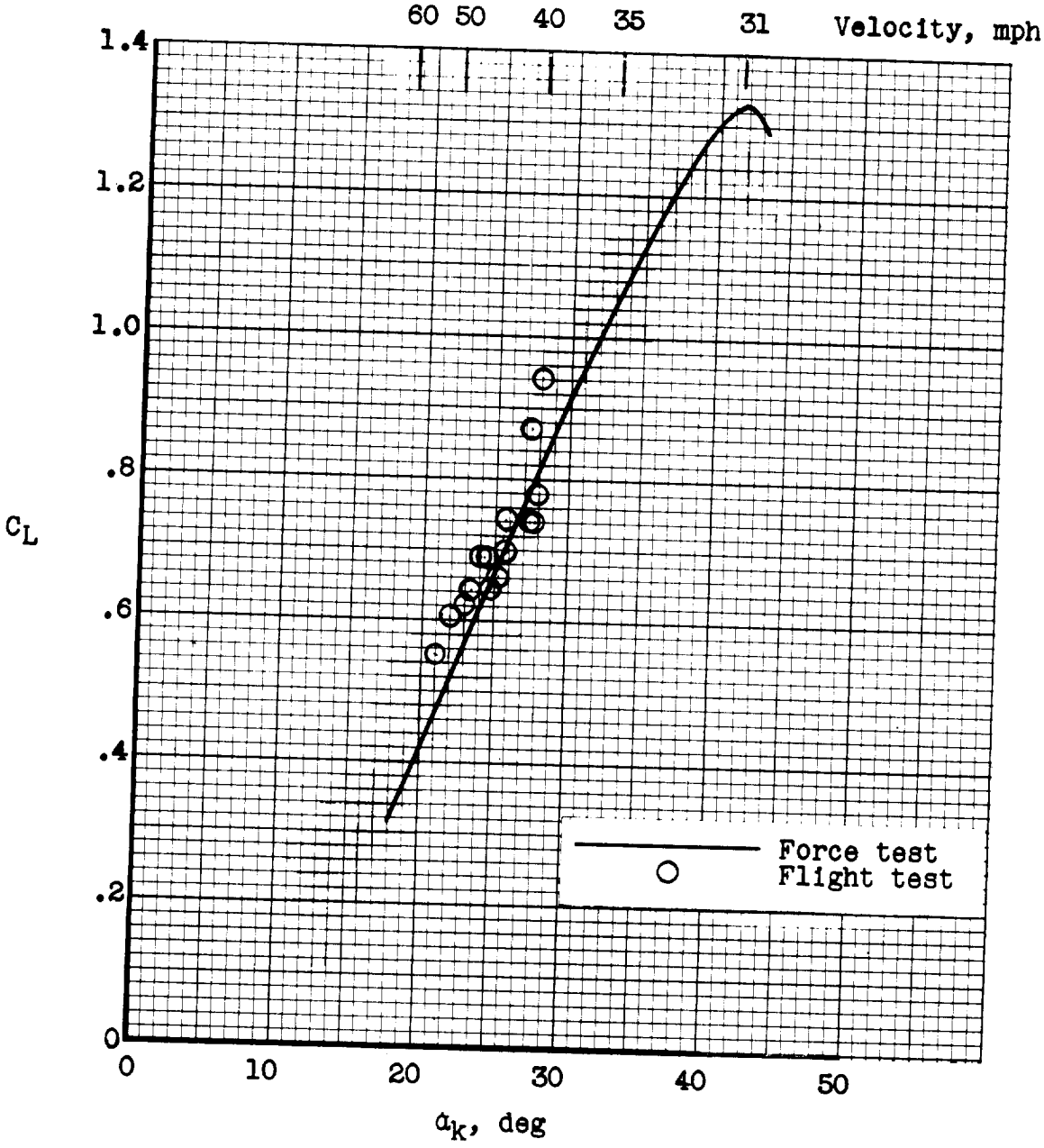

Figure 8.- Comparison of lift characteristics as measured in wind-tunnel tests and Ryan flight tests of the airplane. Airspeeds were estimated for 1,840 pounds.

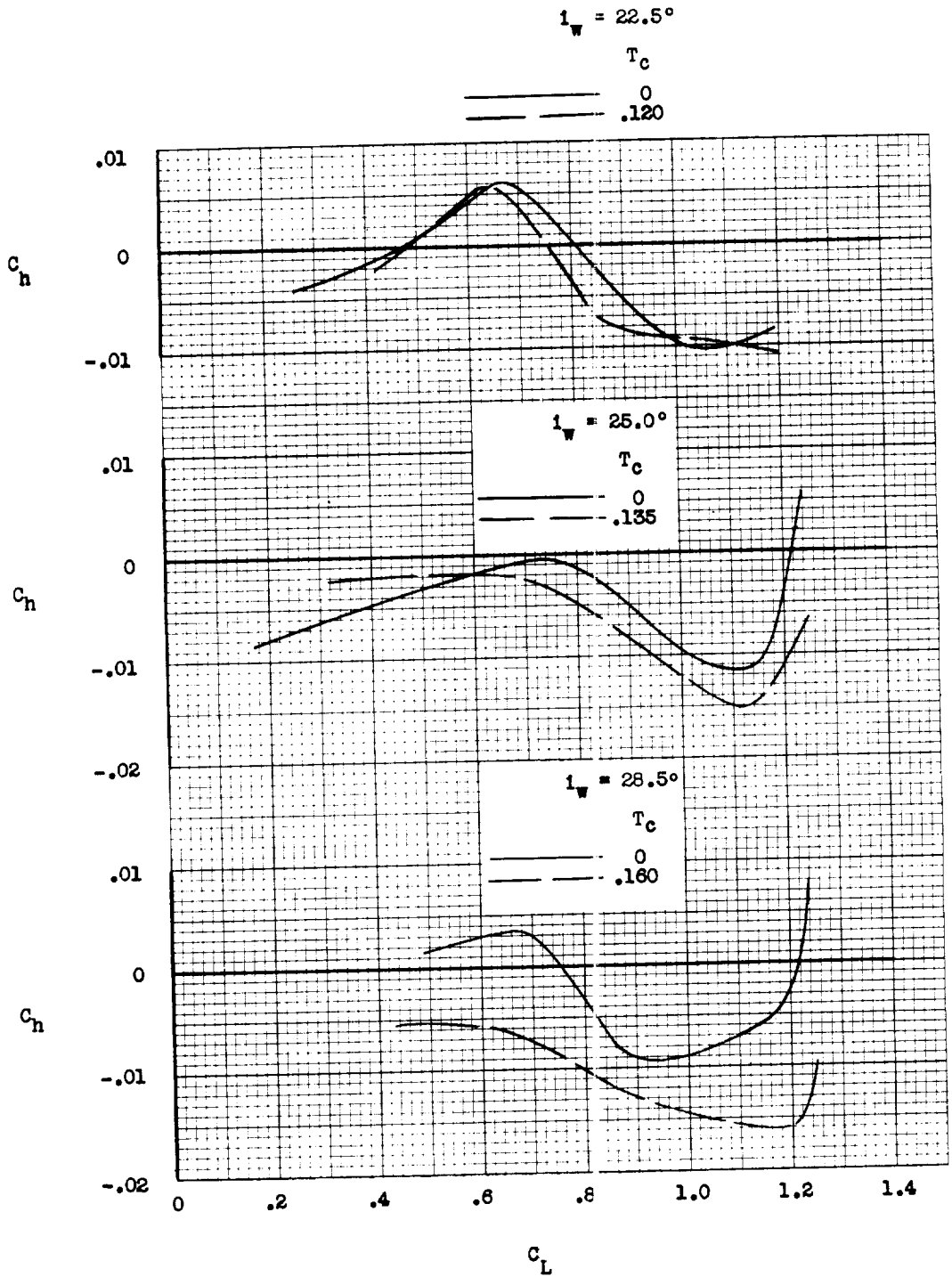

Figure 9.- Hinge-moment characteristics of the wing in pitch measured about the pivot for constant dynamic-pressure conditions.

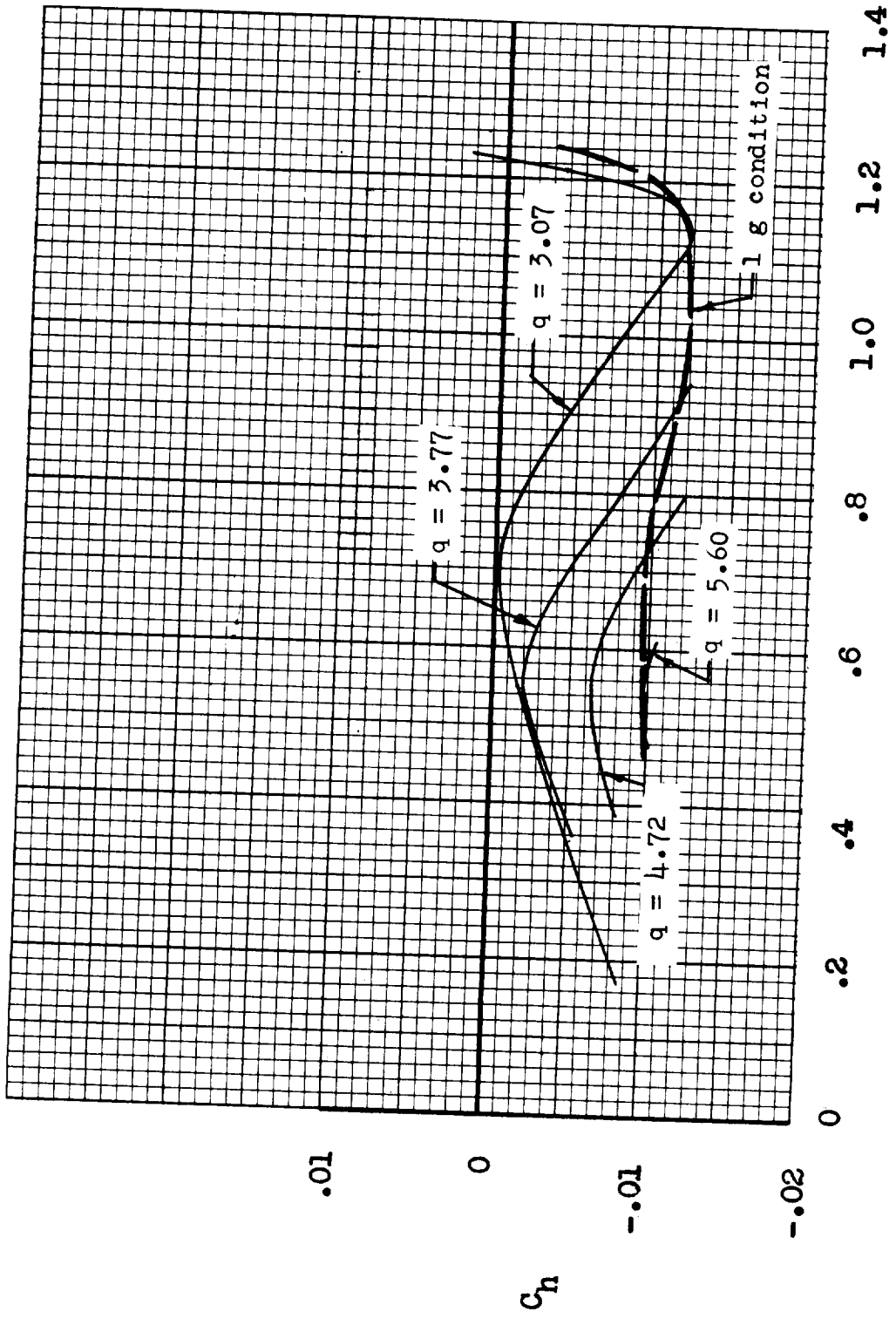

Figure 10.- Effect of dynamic pressure on the hinge-moment characteristics of the wing in pitch.
$T_c = 0$.

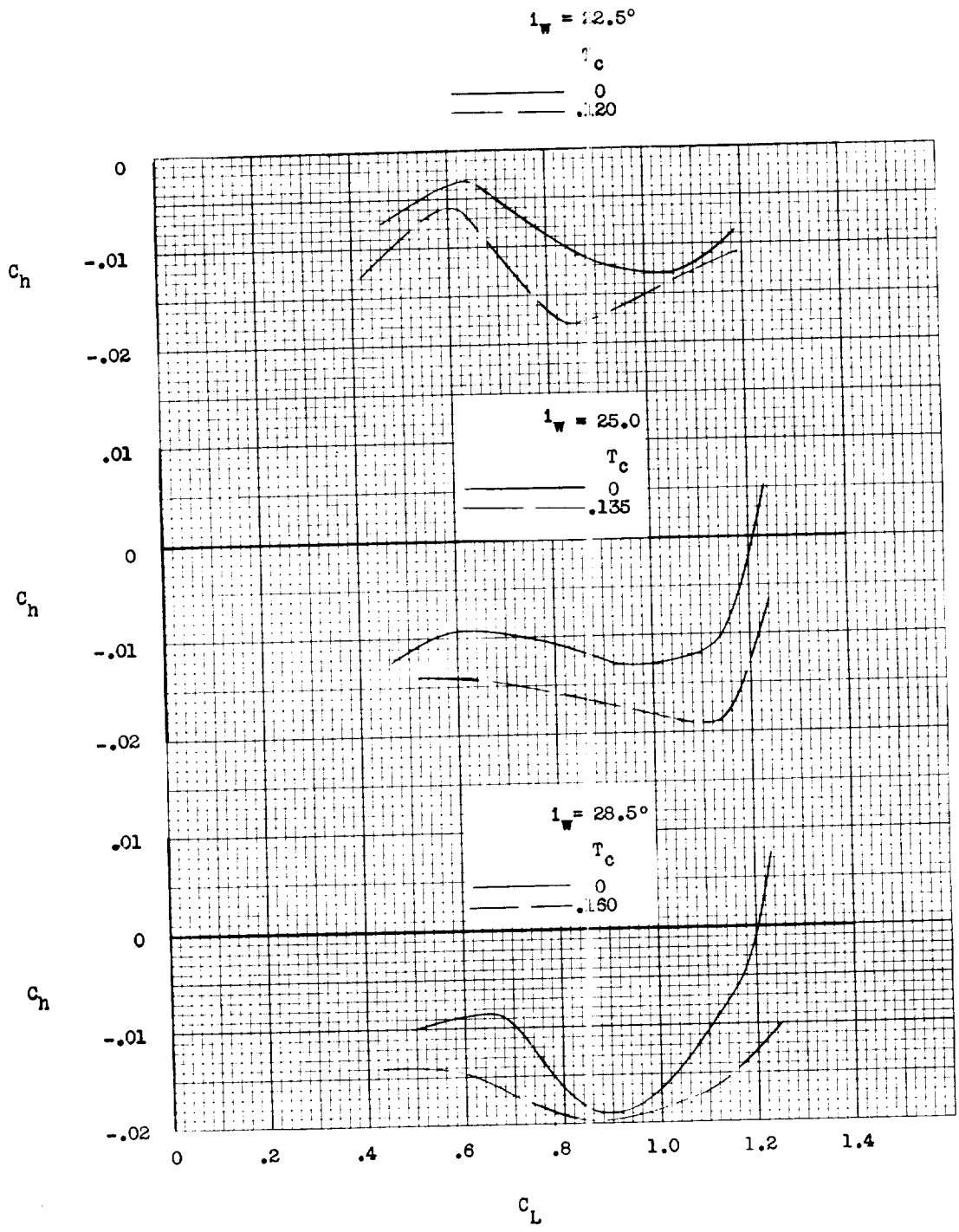

Figure 11.- Hinge-moment characteristics of the wing in pitch corrected for 1 g condition.

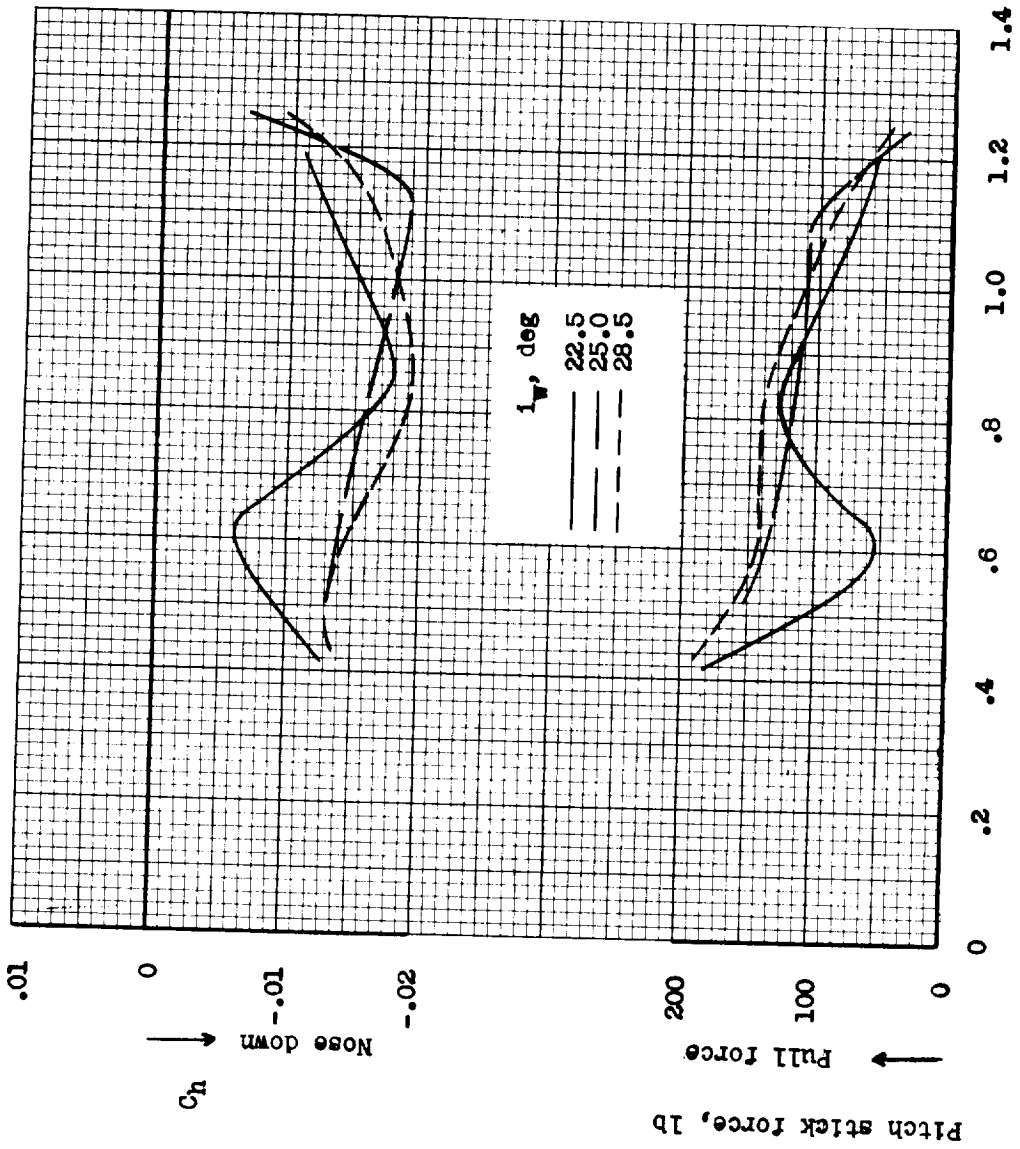

Figure 12.- Hinge-moment characteristics of the wing in pitch (data from fig. 11) and corresponding pitch stick forces for three different wing incidences. Power on.

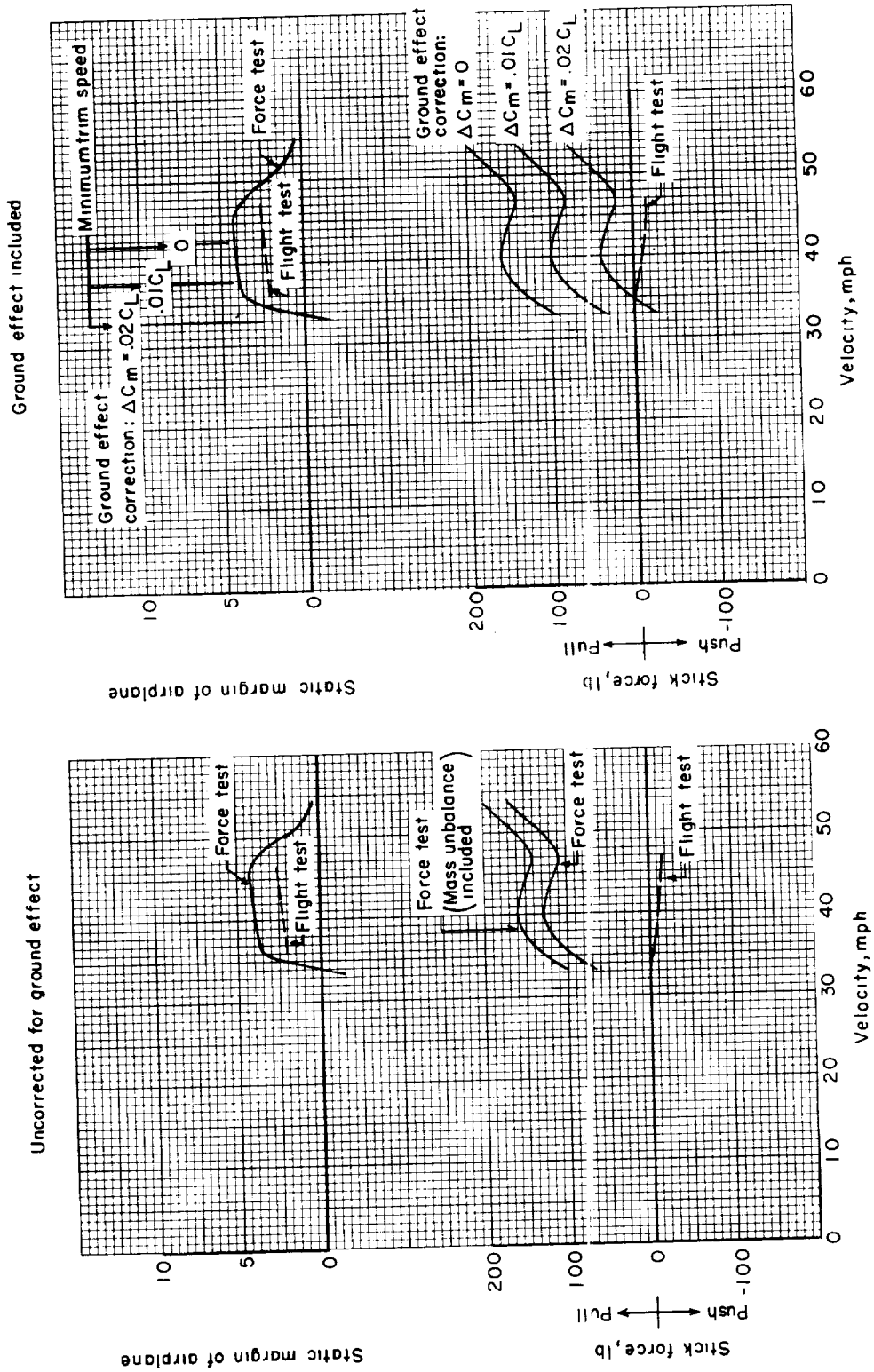

Figure 13.- Comparison of static margin and pitch stick forces as measured in wind-tunnel tests and Ryan flight tests of the airplane. Power on.

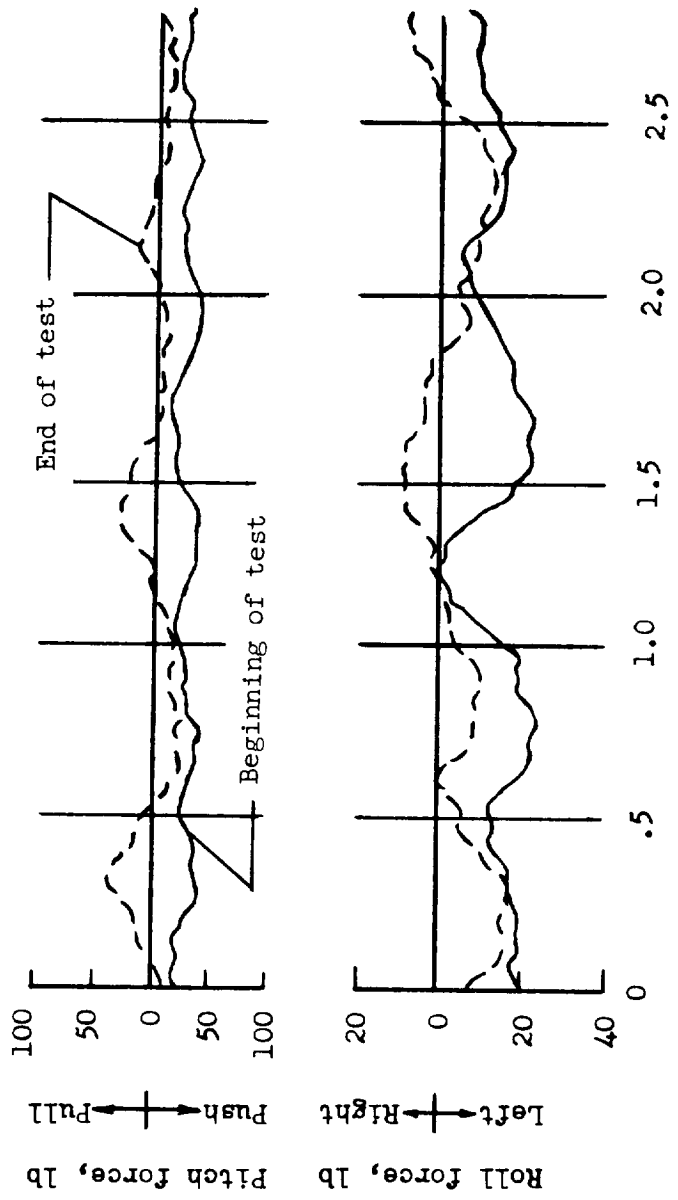

Figure 14.- Time history of control forces measured in the tunnel tests for constant dynamic-pressure conditions. $i_w = 25°$; $T_c = 0$.

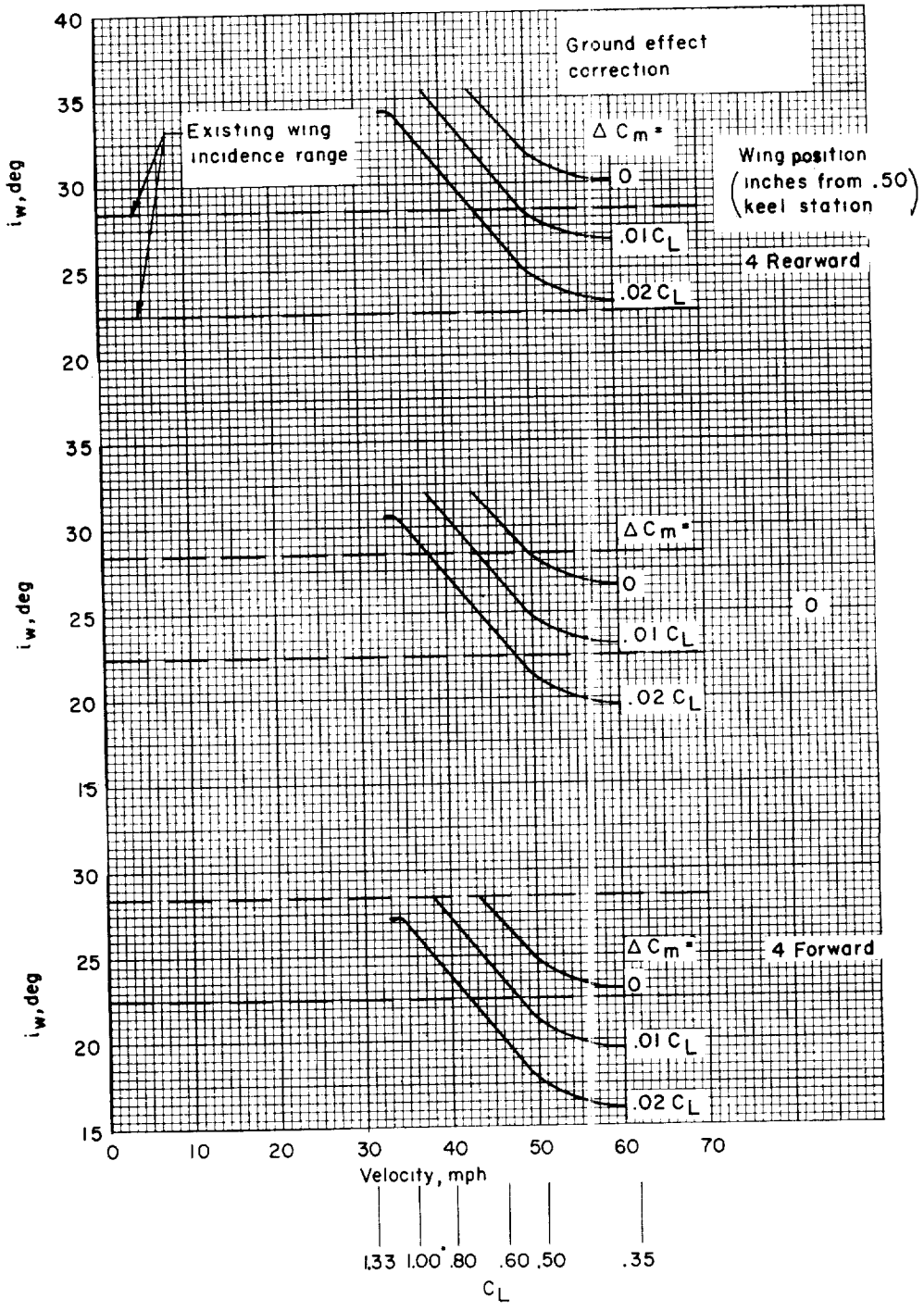

Figure 15.- Estimated angle of incidence required for pitch trim with several different values of ground effect included.

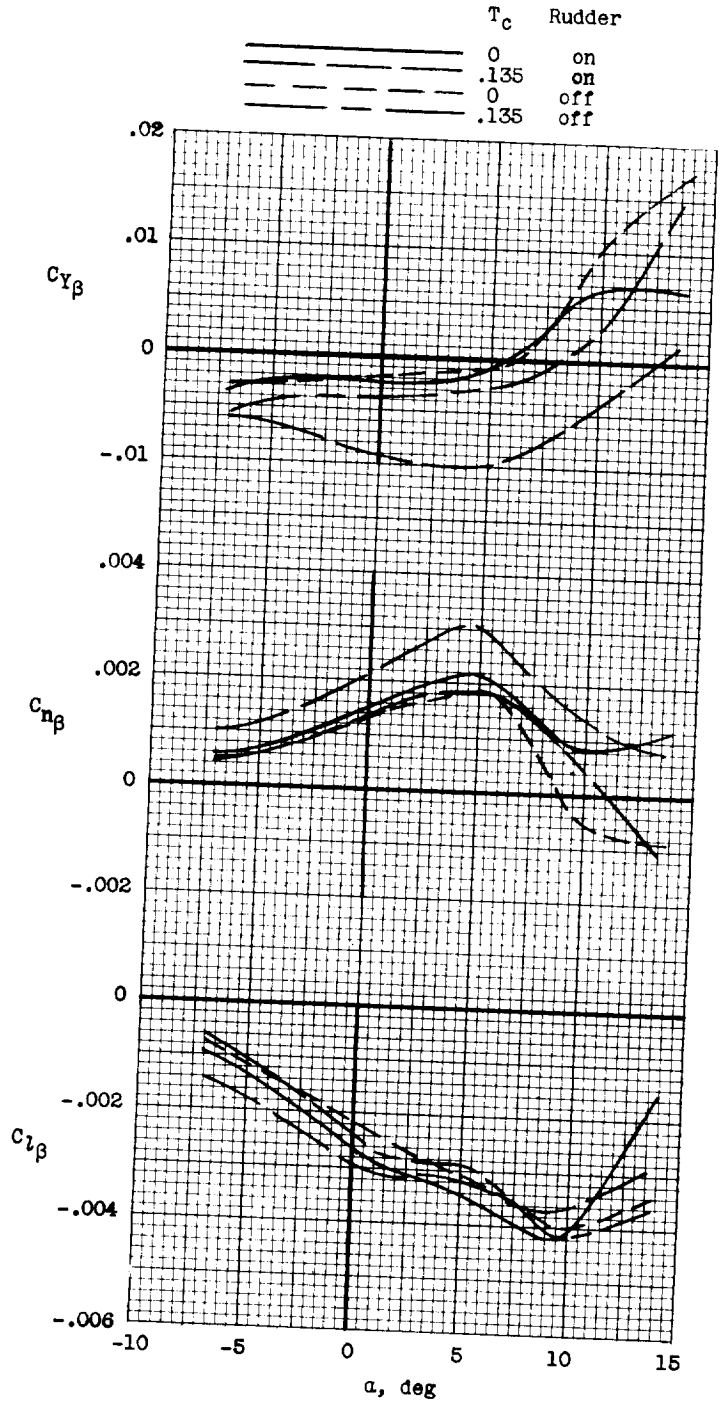

Figure 16.- Effect of power and rudder on static lateral-stability parameters of the airplane. $i_w = 25°$.

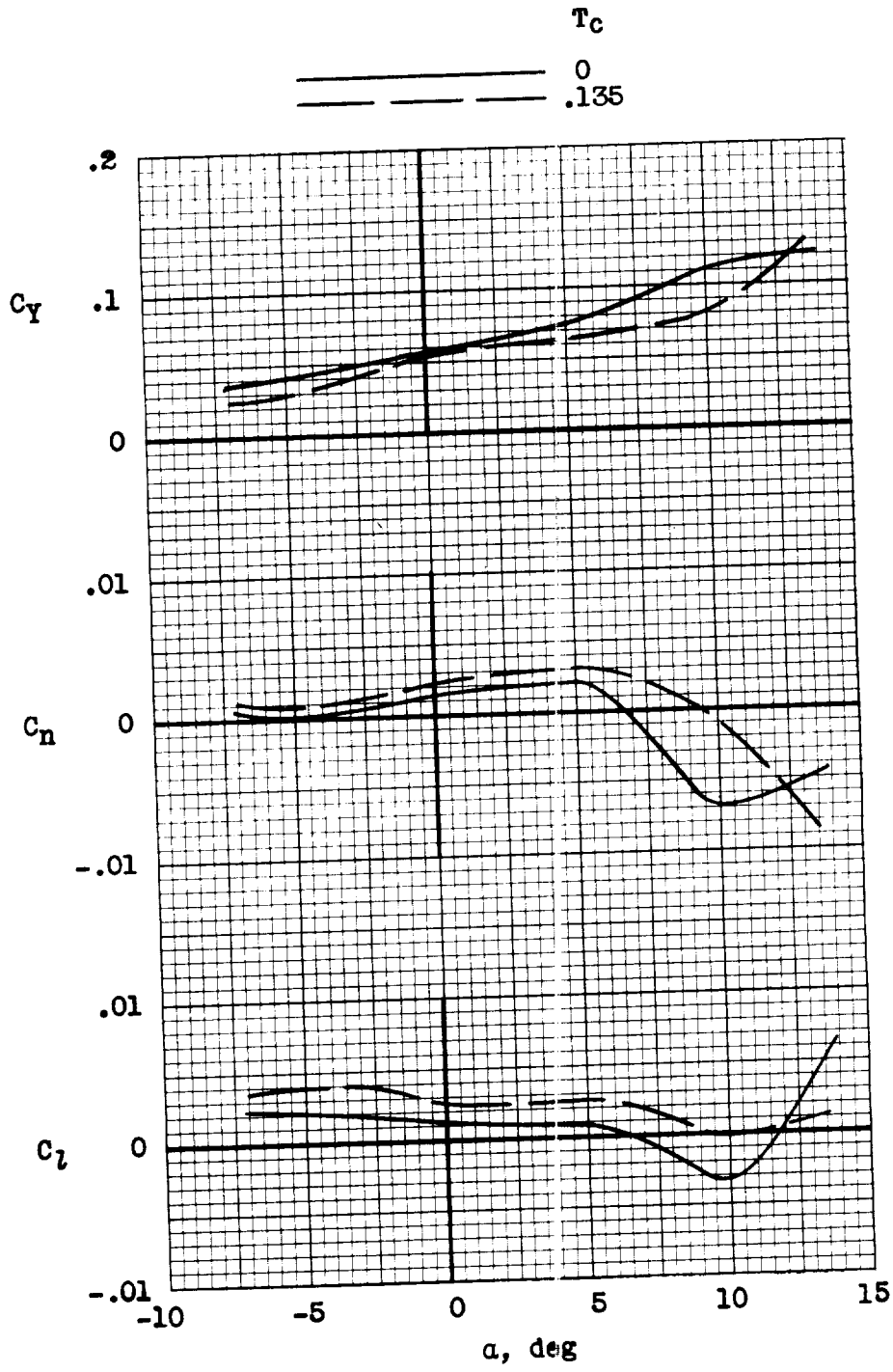

Figure 17.- Incremental lateral force and moments produced by 5° of wing bank. $i_w = 25°$.

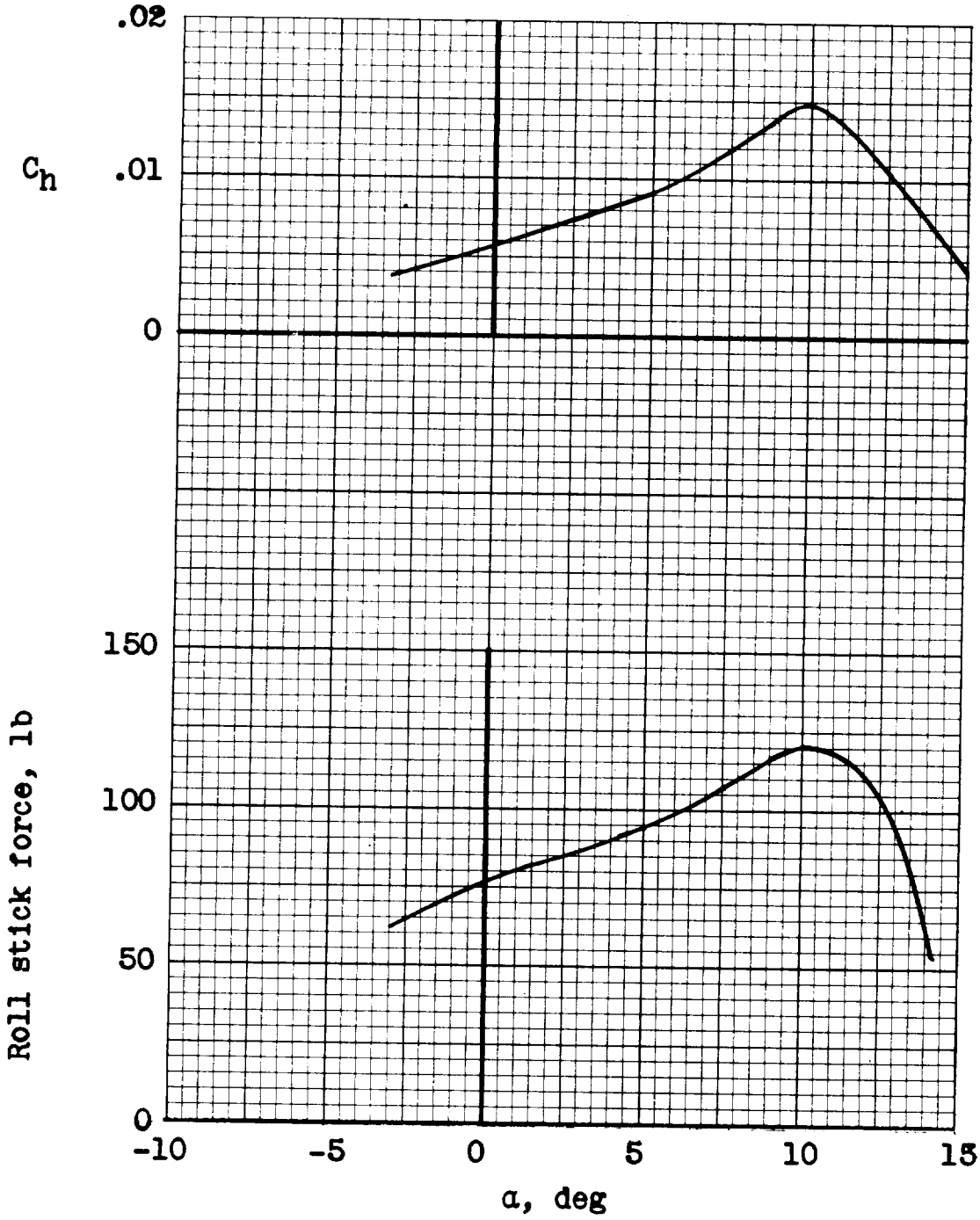

Figure 18.- Roll hinge-moment coefficients of the wing about wing pivot and corresponding roll stick forces produced by 5° of wing bank. i_w = 25°; T_c = 0.

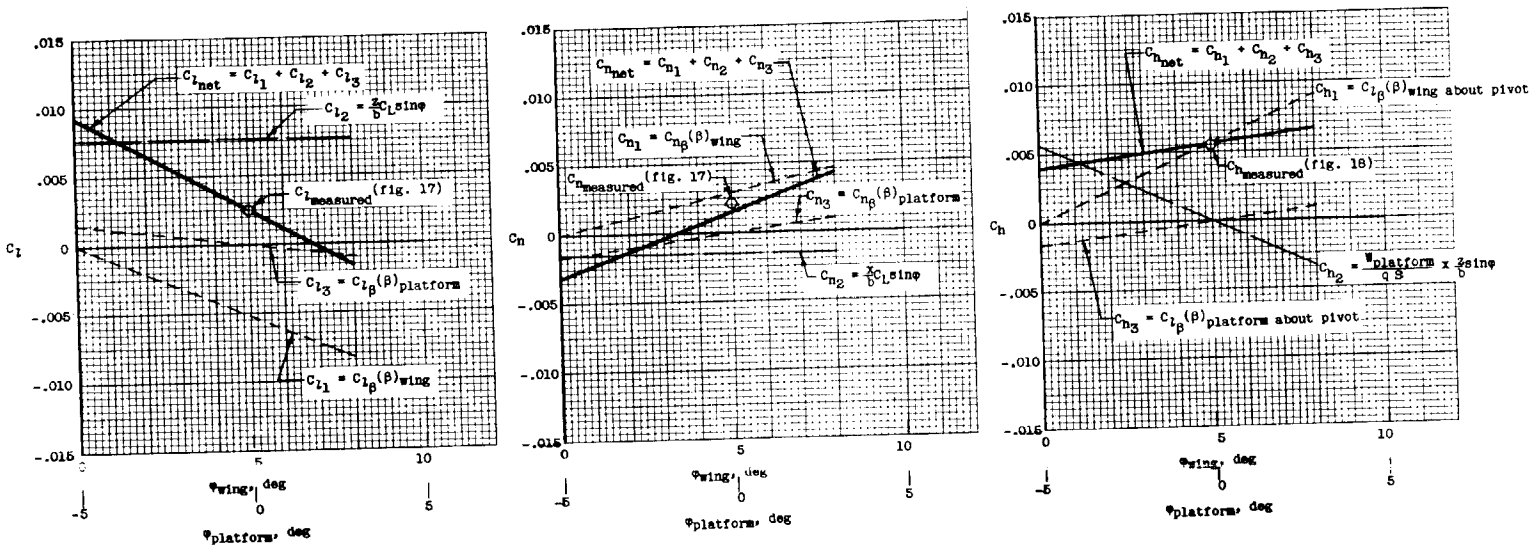

Figure 19.- Estimated incremental yawing- and rolling-moment and hinge-moment coefficients as obtained by various proportions of wing and platform bank angle (relative bank angle between wing and platform held constant at 5°). $i_w = 25°$; $\alpha = 0°$.

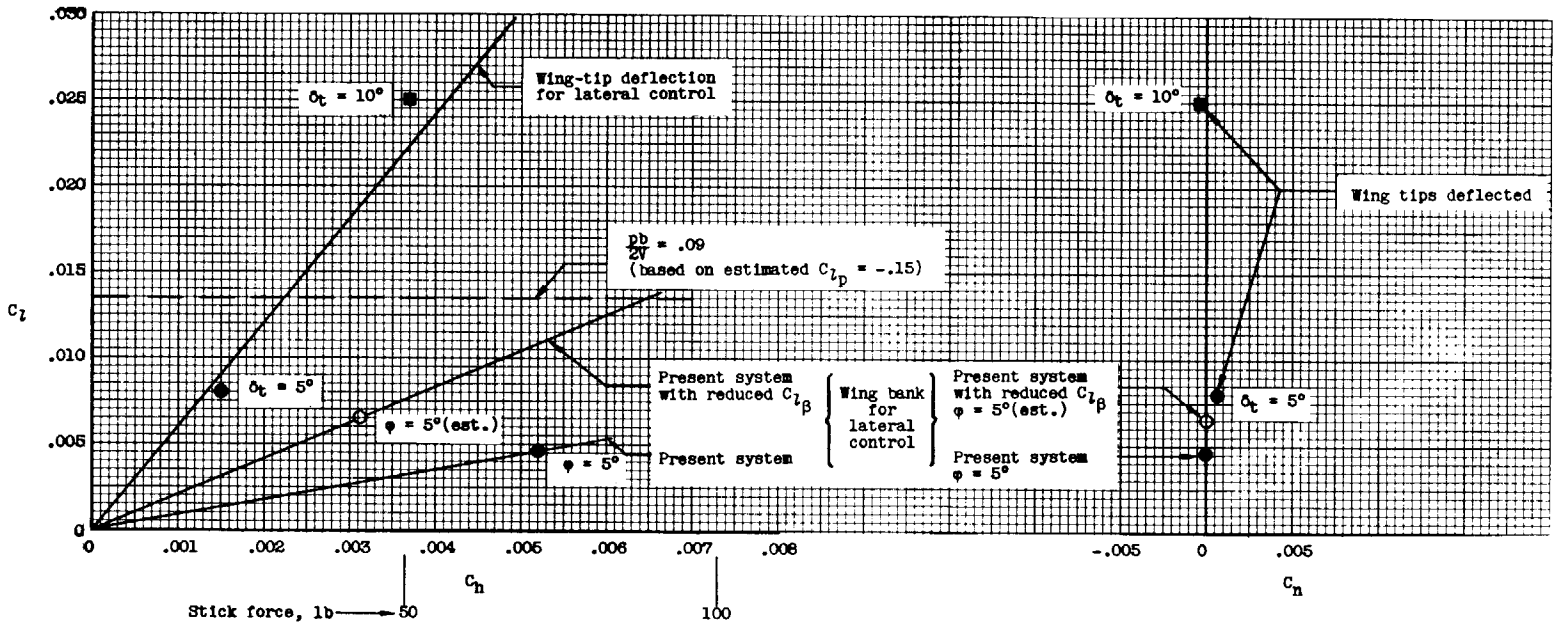

(a) Rolling-moment and hinge-moment relationship.

(b) Rolling-moment and yawing-moment relationship.

Figure 20.- Summary of the existing lateral control characteristics of the airplane and comparison with the characteristics of a system using wing-tip deflection for lateral control. $i_w = 25°$; $\alpha = 0°$; gross weight = 1,840 pounds.

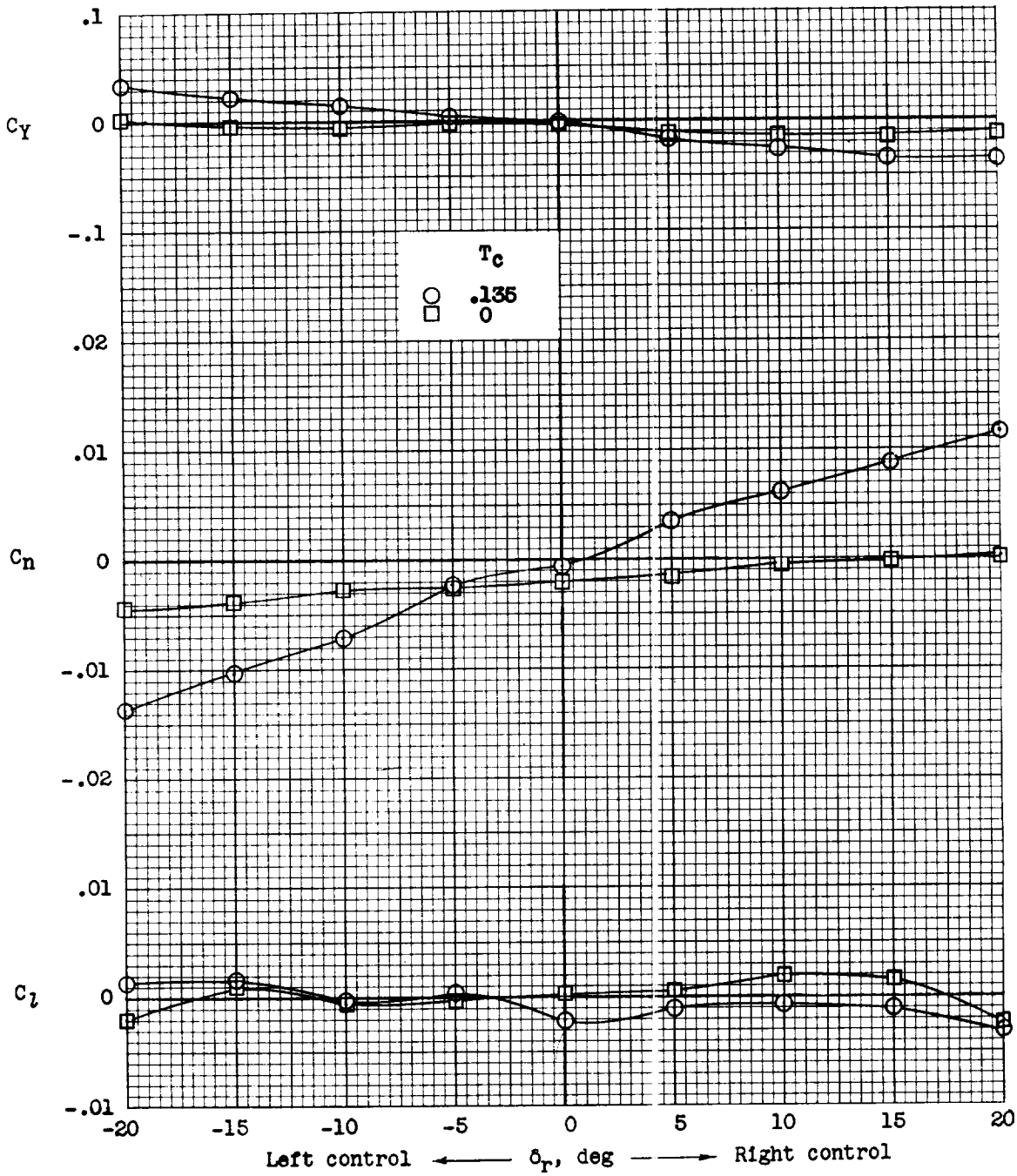

Figure 21.- Effect of power-on rudder control. $\alpha = 0^\circ$; $i_w = 25^\circ$.